

<https://doi.org/10.3799/dqkx.2020.286>



东昆仑巴隆地区晚三叠世石英闪长岩成因:U-Pb年代学、地球化学及Sr-Nd-Hf同位素制约

黄啸坤¹,魏俊浩^{1*},李欢¹,陈梦婷¹,王艺龙^{2,3},李国猛¹,闫茂强¹,张新铭¹

1. 中国地质大学资源学院,湖北武汉 430074

2. 辽宁省地质勘查院有限责任公司,辽宁大连 116100

3. 高分辨率对地观测系统辽宁地质资源环境应用与服务中心,辽宁大连 116100

摘要:花岗岩的研究对于反演造山带下地壳物质组成、造山作用深部动力学过程具有重要意义。对位于东昆仑造山带东段的巴隆石英闪长岩开展了锆石U-Pb年代学、Hf同位素地球化学、全岩主微量元素地球化学和Sr-Nd同位素地球化学研究,以探讨其岩石成因和构造背景。岩体LA-ICP-MS锆石U-Pb定年结果为229.5±1.4 Ma,为晚三叠世岩浆活动产物。全岩SiO₂含量为59.86%~61.83%,显示高Na₂O(3.38%~3.55%)和Al₂O₃(16.38%~17.03%)特征,Na₂O/K₂O为1.25~1.39,Mg#为50.1~52.3,属高钾钙碱性系列。稀土元素标准化图呈右倾,具有较弱的负铕异常(δ Eu=0.71~0.82),微量元素蛛网图显示富集大离子亲石元素(LILE),显著亏损高场强元素(HFSE)。石英闪长岩的高Sr($474\sim609\times10^{-6}$)、Sr/Y(32.31~40.86)、(La/Yb)_N(13.34~15.32)和低Yb($1.34\sim1.75\times10^{-6}$)、Y($13.40\sim15.60\times10^{-6}$)含量与埃达克质岩石特征相似。全岩(⁸⁷Sr/⁸⁶Sr)_i为0.708186~0.708428,ε_{Nd}(t)为-5.75~-5.27,对应的二阶段模式年龄t_{DM2}(Nd)为1432~1471 Ma;ε_{Hf}(t)为-5.2~-3.2,t_{DM2}(Hf)为1305~1420 Ma。岩相学、元素地球化学和Sr-Nd-Hf同位素结果揭示石英闪长岩起源于加厚下地壳的部分熔融,并混有幔源岩浆。构造判别图解显示巴隆石英闪长岩体形成于后碰撞伸展构造环境。东昆仑与巴颜喀拉地体的陆陆碰撞导致板片断离,软流圈物质上涌,使富集地幔熔融并底侵下地壳,下地壳部分熔融形成巴隆石英闪长岩。

关键词:石英闪长岩,晚三叠世,壳幔混合作用,后碰撞,东昆仑造山带;岩石学;地球化学。

中图分类号: P581

文章编号: 1000-2383(2021)06-2037-20

收稿日期: 2020-04-27

Zircon U-Pb Geochronological, Elemental and Sr-Nd-Hf Isotopic Constraints on Petrogenesis of Late Triassic Quartz Diorite in Balong Region, East Kunlun Orogen

Huang Xiaokun¹, Wei Junhao^{1*}, Li Huan¹, Chen Mengting¹, Wang Yilong²⁺³, Li Guomeng¹, Yan Maoqiang¹, Zhang Xinming¹

1. School of Earth Resources, China University of Geosciences, Wuhan 430074, China

2. Geological Exploration Institute of Liaoning Province, Dalian 116100, China

3. Liaoning Province High-Resolution Observation System Application and Service Center of Geological Resources and Environmental, Dalian 116100, China

基金项目:国家自然科学基金项目(No.41772071)。

作者简介:黄啸坤(1992—),男,博士研究生,矿产普查与勘探专业。ORCID:0000-0002-5869-8216. E-mail:hxkshaw@163.com

*通讯作者:魏俊浩,E-mail:junhaow@163.com

引用格式:黄啸坤,魏俊浩,李欢,等,2021.东昆仑巴隆地区晚三叠世石英闪长岩成因:U-Pb年代学、地球化学及Sr-Nd-Hf同位素制约.

地球科学,46(6):2037-2056.

Abstract: The study of granite is of great significance to the inversion of the material composition of the lower crust and the deep dynamic process of orogeny. The quartz diorite in Balong region is located in the east of the East Kunlun orogen. In this paper, it presents LA-ICP-MS zircon U-Pb age for the Balong quartz diorite to determine precisely the time of the magmatism, and also presents geochemical, Sr-Nd-Hf isotope data for the Balong quartz diorite to constrain the petrogenesis and tectonic setting. The LA-ICP-MS U-Pb analyses of zircon yielded a weighted mean age of 229.5 ± 1.4 Ma, indicating that it was emplaced in the Late Triassic. The quartz diorites have contents of SiO_2 (59.86%–61.83%), Na_2O (3.38%–3.55%), Al_2O_3 (16.38%–17.03%) with $\text{Na}_2\text{O}/\text{K}_2\text{O}$ ratios ranging from 1.25 to 1.39 and $\text{Mg}^{\#}$ values ranging from 50.1 to 51.2. They are characterized by high silicon and belonging to the high-potassium-calcium-alkaline rock. Meanwhile, they are enriched in large ion lithophile elements (LILEs) and depleted in high field strength elements(HFSEs). In addition, the quartz diorite shows characteristics of high Sr/Y (32.31–40.86) and $(\text{La/Yb})_{\text{N}}$ (13.34–15.32) and low contents of Yb (1.34×10^{-6} – 1.75×10^{-6}) and Y (13.40×10^{-6} – 15.60×10^{-6}). These features indicate that the quartz diorite is similar to adakite. All rock samples are enriched in large ion lithophile elements and light rare earth elements, but depleted in high field strength elements. The $(^{87}\text{Sr}/^{86}\text{Sr})_t$ ratios range from 0.708 186 to 0.708 428, $\epsilon_{\text{Nd}}(t)$ values range from –5.75 to –5.27 with corresponding two-stage Nd model ages ranging from 1 432 to 1 471 Ma. The $\epsilon_{\text{Hf}}(t)$ values are from –5.2 to –3.2 and two-stage Hf model ages rang from 1 305 to 1 420 Ma. Integrated geological, geochemical and isotopic data suggest that the quartz diorite from Balong region is most likely generated via partial melting of thickened mafic lower continental crust and with subordinate mantle-derived basic magma. In combination with the tectonic evolution of the East Kunlun orogenic belt and the geochronological and geochemical characteristics of contemporary intrusive rocks, it is concluded that the quartz diorite from Balong region was formed in post-collisional extensional tectonic environment. Slab break-off, triggered by continuous collision between the Bayanhar block and EKOB, led to underplating of basic magma formed by partial melting of enriched mantle. The quartz diorite from Balong region was formed by partial melting of lower crust.

Key words: quartz diorite; Late Triassic; crust-mantle mixing; post-collision; East Kunlun; petrology; geochemistry.

东昆仑造山带地处柴达木盆地以南,是中央造山系的重要组成部分(图1a)(杨经绥等,2010).在长期的地质演化过程中,东昆仑地区经历了包括洋陆转换、弧—弧和弧—陆碰撞在内的复杂多样的构造活动,形成了早古生代到新生代的巨型岩浆带(王艺龙等,2018),并以海西—印支期花岗岩体的分布最广。

东昆仑地区出露的晚古生代—中生代岩浆岩与古特提斯洋的演化密切相关(莫宣学等,2007).东昆仑古特提斯对应的蛇绿岩在空间上沿昆南断裂分布,构成了昆南—阿尼玛卿蛇绿岩带(杨经绥等,2004),该带上德尔尼玄武岩(345.3 Ma, Chen et al., 2001; 308.2 Ma, 杨经绥等,2004)、布青山地区蛇绿岩(332.8 Ma; 刘战庆等,2011)的研究均有效揭示了古特提斯洋在早石炭世已开始扩张.具有岛弧性质的277.76 Ma小庙岩墙群和262~277 Ma下大武组岛弧玄武岩的报道暗示古特提斯洋在早中二叠世开始俯冲(Liu et al., 2014; 熊富浩,2014).随着晚二叠世大规模的洋壳俯冲,东昆仑地区形成了广泛分布的花岗质侵入岩.该背景下形成的侵入岩往往为富含暗色微粒包体的钙碱性—高钾钙碱性I型花岗岩,是俯冲作用下壳幔相互作用的产物(Xiong et al., 2012, 2014; 胡朝斌等,2018; 李瑞保等,2018).

然而,古特提斯洋的闭合时间仍然存在争议,

主要观点如下:(1) Huang et al.(2014)针对东昆仑地区240~260 Ma花岗岩类开展研究,认为古特提斯洋的闭合发生于晚二叠世.(2) Chen et al.(2017)、Kong et al.(2020)和 Xiong et al.(2014)认为东昆仑地区248~251 Ma花岗岩类形成于同碰撞阶段, 214~238 Ma花岗岩类形成于后碰撞阶段, 洋壳的俯冲作用在237 Ma结束.Zhao et al.(2020)通过研究沟里坑的弄舍花岗岩、流纹岩认为俯冲发生于240~255 Ma, 碰撞发生于225~240 Ma.(3) Roger et al.(2003)和 Ding et al.(2014)分别报道了缝合带花岗岩(217 Ma, 207 Ma)和五龙沟地区的黄龙沟闪长岩(215 Ma),认为古特提斯直到晚三叠世才关闭.由此可见,关于古特提斯洋的闭合时间还需要更多的证据进行判断.

埃达克岩最早指俯冲洋壳熔融形成的一套具有“高Sr含量、高La/Yb与Sr/Y比值,亏损重稀土元素与Y”等独特的地球化学特征的新生代岛弧火山岩(Defant and Drummond, 1990),后将具有埃达克岩地球化学组成特征的火成岩统称为“埃达克质岩”(许继峰等,2014).埃达克质岩的地球动力学意义在于它是深部地壳熔融形成的,可以更为明确指示俯冲消减事件和地壳加厚作用(张旗等,2003),它能有效反映岩石成因、岩浆源区、构造背景与区域地质演化事件.

因此,本文选取巴隆地区具有埃达克质特征的石英闪长岩为研究对象,开展LA-ICP-MS锆石U-Pb年代学、岩石学、岩石地球化学及同位素地球化学分析,探讨岩石成因及成岩构造背景,对古特提斯洋的闭合时间这一争议性问题提供重要佐证,以期为东昆仑地区古特提斯构造演化提供参考及制约依据。

1 地质背景与岩石学特征

东昆仑造山带位于古亚洲构造域与特提斯构

造域的结合部位,经历了与原特提斯洋和古特提斯洋演化相关的两期重要的构造岩浆演化事件(李文渊等,2011;莫宣学等,2007;许志琴等,2013)。东昆仑造山带内构造线总体呈近北西向展布,昆中断裂带和昆南断裂带横贯东昆仑地区,并将该地区划分为昆北地体、昆南地体等构造单元(图1b)。以花岗岩为主体的侵入岩在东昆仑造山带东段广泛分布,具有多成因性和区域成带性特点,受区域构造的控制明显。

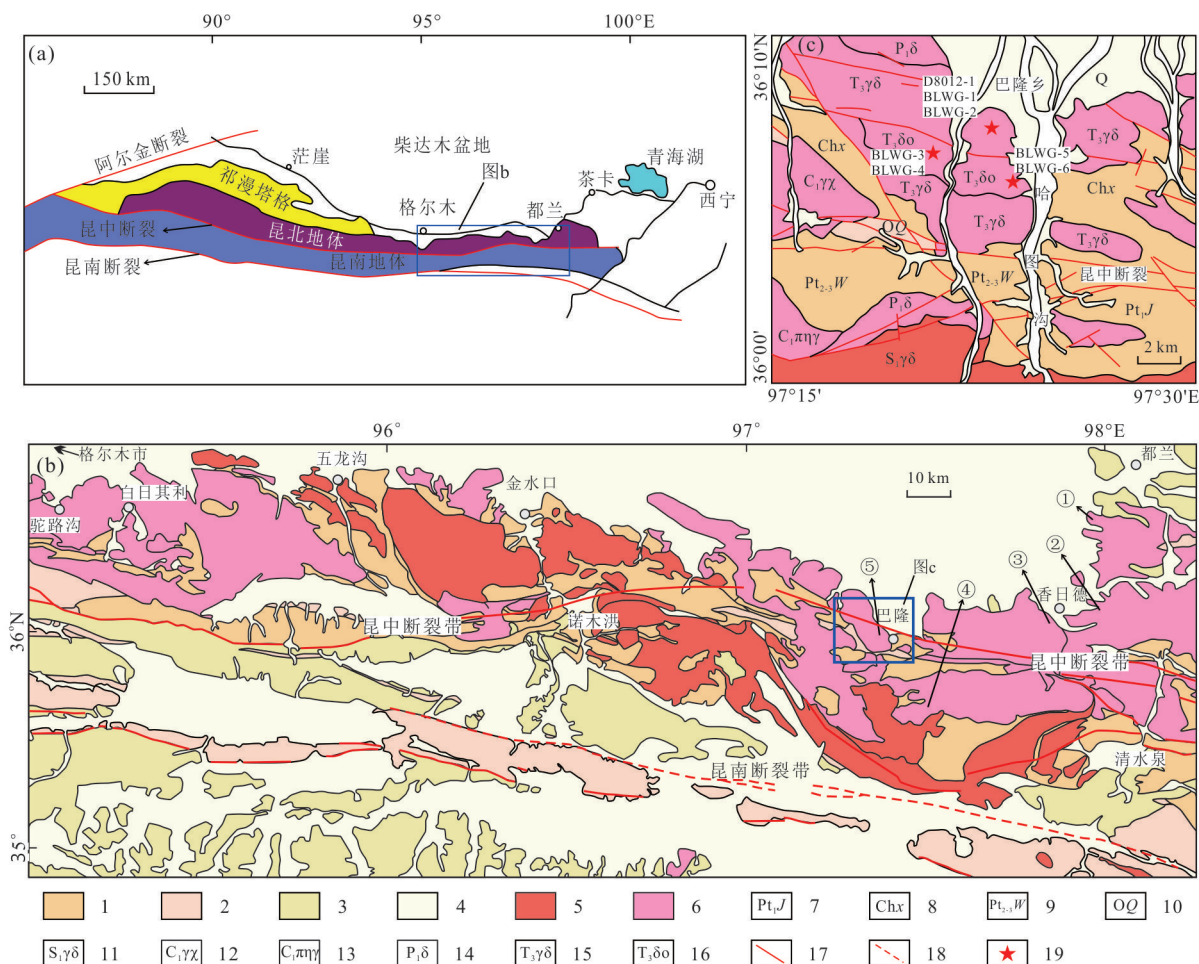


图1 东昆仑构造单元划分图(a),东昆仑地区地质简图(b)及巴隆地区地质简图(c)

Fig.1 Geotectonic framework (a), geological map of the East Kunlun orogen belt (b) and simplified geological map of the Ba-long region (c)

图a据Hu *et al.*(2016);图b修编自Zhang *et al.*(2014);图c修编自1:5万巴隆乡幅地质矿产图;区域上晚三叠世岩浆岩研究概况:①220 Ma都兰花岗闪长岩(Shao *et al.*,2017);②223.6 Ma香日德斑状花岗闪长岩(Xiong *et al.*,2014);③223.2 Ma香日德二长花岗岩,220.6 Ma香日德花岗闪长岩(罗明非等,2014);④218.3 Ma科科鄂阿龙石英闪长岩(陈国超等,2013a),225 Ma和勒冈西里可特花岗闪长岩(陈国超等,2013b);⑤222 Ma小诺木洪花岗闪长岩(夏锐等,2014),215.6 Ma瑙木浑沟闪长玢岩(张明东等,2018);1.元古宙地层;2.古生代地层;3.中生代地层;4.新生代地层;5.早古生代侵入岩;6.晚古生代—中生代侵入岩;7.古元古界金水口群;8.长城系小庙组;9.中—新元古界万宝沟群;10.奥陶系祁漫塔格群;11.早志留世花岗闪长岩;12.早石炭世白岗岩;13.早石炭世似斑状二长花岗岩;14.早二叠世石英闪长岩;15.晚三叠世花岗闪长岩;16.晚三叠世石英闪长岩;17.断层;18.推测断层;19.采样位置

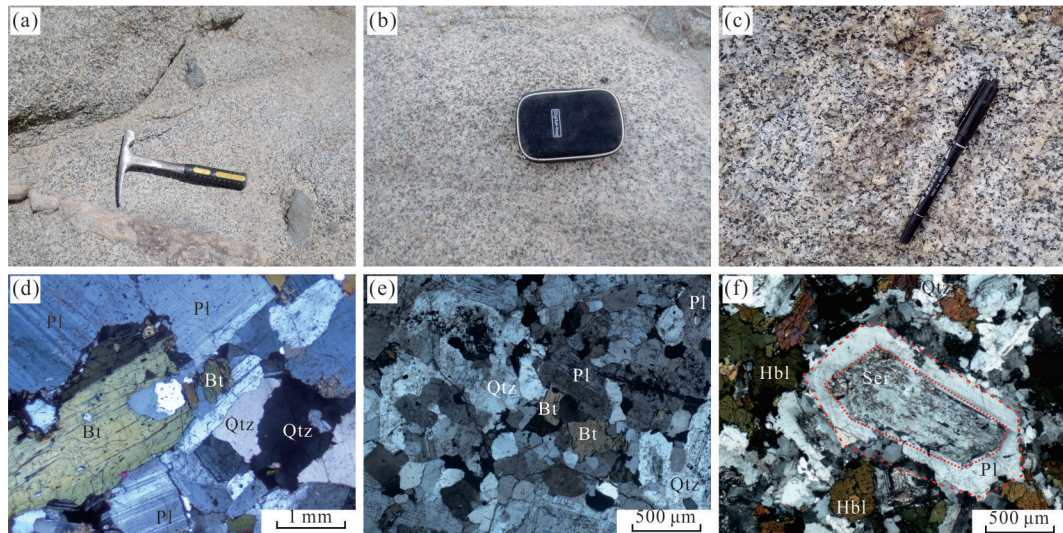


图 2 巴隆石英闪长岩野外露头与镜下显微照片

Fig.2 Sample and microphotographs of the quartz diorite from Balong region

a~c. 地表石英闪长岩露头照片; e~f. 样品显微镜下照片(正交偏光); Pl. 斜长石; Bt. 黑云母; Qtz. 石英; Hbl. 角闪石; Ser. 绢云母化

研究区位于昆仑东段昆中断裂带附近, 区内大面积出露前寒武纪中深变质岩系和早古生代—中生代侵入岩。前寒武纪变质岩系主要包括古元古界金水口群(Pt_1J)、中元古界长城系小庙组(Chx)和中—新元古界万宝沟群($Pt_{2-3}W$)。金水口群分布于研究区东南部, 总体为一套角闪岩相—麻粒岩相深变质岩系, 主要岩石类型为石英片岩、黑云斜长片麻岩、斜长角闪岩及大理岩组合; 小庙组分布于研究区东部, 总体为一套石英质变质岩系, 主要岩石类型为黑云石英片岩、石英岩、角闪片岩及黑云斜长片麻岩; 万宝沟群分布于研究区南西部, 主要为一套浅变质的碎屑岩、火山岩和碳酸盐岩组合。另外, 研究区内还零星出露由砂岩、中基性夹基性火山岩、火山碎屑岩组成的奥陶系祁漫塔格群(OQ)。

早古生代侵入岩分布于研究区西部、南部, 岩性主要为花岗闪长岩、似斑状二长花岗岩、闪长岩、白岗岩, 晚古生代—中生代侵入岩分布于研究区北部、中部, 岩性主要为花岗闪长岩、石英闪长岩等。

巴隆石英闪长岩体出露于巴隆村南部, 岩体出露面积约 15 km^2 , 岩体内部岩性单一。本次研究分别在 3 处地点开展了采样工作, 按照新鲜、无蚀变的原则采集了 7 件样品, 各样品采样地均有一定距离。共采集锆石 U-Pb 定年样品 1 件(D8012-1; N 35.96° , E 97.38°), 岩石地球化学样品 6 件, 采样位置如图 1c。

石英闪长岩新鲜面呈灰白色, 中粒—中细粒结构, 块状构造, 各标本矿物粒度变化不大, 介于 1~

5 mm(图 2a~2c)。主要矿物组成为斜长石(60%), 石英(12%~15%), 黑云母(10%), 钾长石(8%~10%), 角闪石(3%~5%), 副矿物为磷灰石、锆石、榍石等(图 2d~2f)。斜长石多呈自形一半自形板状、板柱状, 发育聚片双晶, 双晶纹疏密不一。斜长石环带结构发育(图 2f), 指示成岩时物理化学环境可能存在突变。钾长石呈自形一半自形板状, 颗粒较大, 格子双晶发育。石英呈他形粒状充填于斜长石、角闪石间隙。角闪石呈柱状, 发育有两组解理。黑云母呈薄片状分布于岩石中。磷灰石多呈针状分布于斜长石中。岩体中发育暗色微粒包体(图 2a), 包体多呈椭球状, 主要为镁铁质, 与寄主岩体多呈截然的接触关系, 灰黑色, 边部可见冷凝边, 矿物成分主要为斜长石、角闪石、黑云母及石英。

2 分析方法

2.1 锆石 LA-ICP-MS U-Pb 定年和 Hf 同位素分析

用于锆石 LA-ICP-MS 定年的样品(D8012-1)采自巴隆乡南部哈图沟口西侧的新鲜露头, 样品由河北省区域地质调查研究所完成破碎, 经重磁分选后选择晶型完好并且纯净透明的锆石制靶, 并在中国地质大学(武汉)地质过程与矿产资源国家重点实验室(GPMR)进行透射光、反射光和阴极发光(CL)照相。

锆石 U-Pb 同位素分析在 GPMR 激光剥蚀等离子质谱仪(LA-ICP-MS)上完成, 激光剥蚀系统为

GeoLas2005, ICP-MS 为 Agilent 7500a. 测试选取无裂隙, 无包裹体的锆石, 并在环带清晰的部位布点, 激光束斑直径 $32 \mu\text{m}$. 选用 91500 作为内标对 U-Th-Pb 同位素进行校正, 并选用 GJ-1 作为监测样, 选用 NIST610 作为外标, ^{29}Si 作为内标进行微量元素校正计算, 详细的分析流程及仪器参数参见 (Liu *et al.*, 2008, 2010a, 2010b). 对于实验数据的处理及校正均基于软件 ICPMSData Cal 9.5 完成. 锆石样品的 U-Pb 协和图绘制和加权平均年龄计算均基于软件 Isoplot 3.75 完成(Ludwig, 2003).

锆石 Hf 同位素分析在 GPMR 采用激光剥蚀多接收等离子体质谱仪 (LA-MC-ICP-MS), 激光剥蚀系统和质谱仪与 U-Pb 测试系统一致. Hf 同位素测试点位置与 U-Pb 测试点一致或在同一颗锆石相同环带内, 激光束斑直径为 $44 \mu\text{m}$. 详细的分析流程参照(Hu *et al.*, 2012).

2.2 全岩地球化学测试

在室内详细的岩相学鉴定的基础上选取了 6 件新鲜岩石样品, 切除有蚀变、裂隙部分并清除表面粉尘, 粉碎至 200 目以下, 进行主量元素、微量元素和 Sr-Nd 同位素分析.

主量、微量及稀土元素分析在澳实矿物实验室集团澳实分析监测(广州)有限公司测试. 主量元素采用 ME-XRF26d 方法分析完成. 将一份试样中加入含硝酸锂的硼酸锂—硝酸锂熔融助熔剂, 充分混合后, 高温熔融. 将熔融物倒入铂金模子形成扁平玻璃片后, 使用 X 射线荧光光谱仪分析; 将另一份试样放入马弗炉中, 于 1000°C 灼烧, 冷却后称重. 样品加热前后的重量差即是烧失量. 烧失量的结果和 XRF 测得的元素氧化物结果相加, 即为本方法的加和“total”. 该方法分析精密度控制相对误差小于 5%, 准确度控制相对误差小于 5%.

微量元素分析方法为 ME-MS61, 采用等离子体发射光谱与等离子体质谱 (ICP-AES & ICP-MS) 进行测试. 称取试样于 Teflon 试管中, 然后用硝酸、盐酸、高氯酸、氢氟酸分三个阶段进行消解. 残液用盐酸稀释并定容, 再用等离子体发射光谱与等离子体质谱进行分析. 元素之间的光谱干扰得到矫正后, 即是最后分析结果. 该方法分析精密度控制相对误差小于 10%, 准确度控制相对误差小于 10%.

稀土元素分析方法为 ME-MS81, 采用电感耦合等离子体质谱仪 (ICP-MS) 进行测试. 测试步骤

如下: 往试样中加入硼酸锂 ($\text{LiBO}_2/\text{Li}_2\text{B}_4\text{O}_7$) 熔剂, 混合均匀, 在熔炉中于 1025°C 熔融. 待熔融液冷却后, 用硝酸、盐酸和氢氟酸消解并定容, 然后用等离子体质谱仪分析. 该方法分析精密度控制相对误差小于 10%, 准确度控制相对误差小于 10%.

全岩 Sr-Nd 同位素在武汉地质调查中心测试, 采用热电离质谱仪 Triton 分析, 质谱分析中产生的质量分馏采用 $^{146}\text{Nd}/^{144}\text{Nd}=0.7219$ 进行幂定律校正, Sm、Nd 含量采用同位素稀释法公式计算得到, 整个分析过程用 GBW04419、BCR-2 和 JMC 标准物质分别对全流程和一起进行监控. 获得的 GBW04419 标准测定平均值分别为: $\text{Sm}=3.037 \times 10^{-6}$, $\text{Nd}=10.14 \times 10^{-6}$, $^{143}\text{Nd}/^{144}\text{Nd}=0.512735 \pm 0.000005$, JMC 的 $^{143}\text{Nd}/^{144}\text{Nd}=0.511554 \pm 0.000009$, 与其推荐值在误差范围内完全一致. 全流程 Nd、Sm 空白分别为 4×10^{-11} 和 8×10^{-11} .

3 分析结果

3.1 锆石 U-Pb 年代学

石英闪长岩样品 (D8012-1) 锆石为无色—浅黄色, 以短轴状、等轴状居多, 晶体长度集中于 $150 \sim 300 \mu\text{m}$. CL 图显示样品发育明显的震荡环带 (图 3a). 对韵律环带明显的 20 颗锆石进行了定年测试分析, 结果见表 1. 锆石的 U、Th 含量分别为 $143 \sim 515 \times 10^{-6}$ 和 $78 \sim 215 \times 10^{-6}$, Th/U 值为 $0.42 \sim 0.94$, 与岩浆锆石一致 ($\text{Th}/\text{U} > 0.1$; Griffin *et al.*, 2004). 所有分析数据点都位于谐和线上及附近, $^{206}\text{Pb}/^{238}\text{U}$ 年龄介于 $227 \pm 3 \sim 234 \pm 5 \text{ Ma}$, 加权平均年龄为 $229.5 \pm 1.4 \text{ Ma}$ ($\text{MSWD}=0.30$) (图 3b, 3c), 为晚三叠世岩浆活动的产物.

3.2 岩石地球化学特征

6 件主量元素测试结果见于表 2. 该岩体 SiO_2 含量为 $59.86\% \sim 61.83\%$, 变化范围较小; $\text{Na}_2\text{O}=3.38\% \sim 3.55\%$, $\text{K}_2\text{O}=2.50\% \sim 2.85\%$, 全碱 ($\text{K}_2\text{O}+\text{Na}_2\text{O}$) = $6.03\% \sim 6.40\%$, $\text{Al}_2\text{O}_3=16.38\% \sim 17.03\%$. 样品 FeO^{T} 含量较高 ($4.39 \sim 5.36$), 但 MgO 含量较低 ($2.60\% \sim 3.13\%$), $\text{Mg}^{\#}=50.1 \sim 52.3$. 上述主量元素特征指示巴隆石英闪长岩属于高钾钙碱性系列并具有准铝质特征 (图 4).

稀土元素及微量元素地球化学数据见表 2. 石英闪长岩稀土元素总量为 $115.49 \times 10^{-6} \sim 137.37 \times 10^{-6}$, LREE/HREE = $9.39 \sim 10.50$, 显示轻稀土元素分馏明显, 重稀土元素分馏相对较弱. 球粒陨石标

表 1 巴隆石英闪长岩(D8012-1)锆石 LA-ICP-MS U-Pb 定年分析数据

Table 1 Zircon LA-ICP-MS U-Pb data of the Balong quartz diorite sample (D8012-1)

测试点号	^{232}Th (10^{-6})	^{238}U (10^{-6})	Th/U	U-Th-Pb 同位素比值				年龄(Ma)											
				$^{207}\text{Pb}/^{206}\text{Pb}$	$^{207}\text{Pb}/^{235}\text{U}$	$^{206}\text{Pb}/^{238}\text{U}$	$^{208}\text{Pb}/^{232}\text{Th}$	$^{207}\text{Pb}/^{206}\text{Pb}$	$^{207}\text{Pb}/^{235}\text{U}$	$^{206}\text{Pb}/^{238}\text{U}$	$^{208}\text{Pb}/^{232}\text{Th}$	$^{207}\text{Pb}/^{206}\text{Pb}$	$^{207}\text{Pb}/^{235}\text{U}$	$^{206}\text{Pb}/^{238}\text{U}$	$^{208}\text{Pb}/^{232}\text{Th}$				
D8012-1-1	111	216	0.51	0.0541	0.0028	0.2669	0.0139	0.0362	0.0006	0.0110	0.0004	372	119	240	11	229	4	221	8
D8012-1-2	175	283	0.62	0.0519	0.0028	0.2660	0.0151	0.0369	0.0005	0.0136	0.0004	280	160	239	12	234	3	272	8
D8012-1-3	78	143	0.54	0.0520	0.0044	0.2600	0.0215	0.0369	0.0007	0.0126	0.0005	283	194	235	17	234	5	253	9
D8012-1-4	87	159	0.55	0.0505	0.0033	0.2511	0.0164	0.0362	0.0005	0.0124	0.0004	220	152	227	13	229	3	250	9
D8012-1-5	151	256	0.59	0.0508	0.0032	0.2529	0.0164	0.0361	0.0006	0.0125	0.0004	232	146	229	13	229	4	252	9
D8012-1-6	94	192	0.49	0.0519	0.0031	0.2561	0.0152	0.0364	0.0005	0.0124	0.0004	280	106	232	12	230	3	248	7
D8012-1-7	108	188	0.58	0.0510	0.0025	0.2525	0.0124	0.0364	0.0004	0.0123	0.0003	239	115	229	10	230	3	248	7
D8012-1-8	183	241	0.76	0.0523	0.0033	0.2605	0.0166	0.0360	0.0005	0.0116	0.0003	298	146	235	13	228	3	234	7
D8012-1-9	134	281	0.48	0.0511	0.0025	0.2521	0.0121	0.0359	0.0005	0.0129	0.0004	256	111	228	10	227	3	258	7
D8012-1-10	87	179	0.49	0.0503	0.0027	0.2496	0.0138	0.0362	0.0005	0.0118	0.0004	209	126	226	11	229	3	237	7
D8012-1-11	96	154	0.62	0.0522	0.0032	0.2557	0.0150	0.0362	0.0005	0.0115	0.0004	295	139	231	12	229	3	232	9
D8012-1-12	215	515	0.42	0.0501	0.0019	0.2501	0.0093	0.0360	0.0004	0.0107	0.0002	198	87	227	8	228	2	216	5
D8012-1-13	84	151	0.56	0.0510	0.0050	0.2550	0.0251	0.0363	0.0007	0.0117	0.0006	239	211	231	20	230	4	234	12
D8012-1-14	172	183	0.94	0.0507	0.0036	0.2483	0.0169	0.0360	0.0005	0.0104	0.0003	233	168	225	14	228	3	209	6
D8012-1-15	121	169	0.72	0.0523	0.0035	0.2605	0.0170	0.0364	0.0005	0.0111	0.0004	298	128	235	14	230	3	222	7
D8012-1-16	123	177	0.69	0.0491	0.0030	0.2468	0.0151	0.0364	0.0005	0.0102	0.0003	150	56	224	12	230	3	205	5
D8012-1-17	212	270	0.78	0.0519	0.0025	0.2575	0.0119	0.0360	0.0005	0.0108	0.0003	280	111	233	10	228	3	218	5
D8012-1-18	195	254	0.77	0.0510	0.0023	0.2528	0.0114	0.0359	0.0004	0.0096	0.0003	239	106	229	9	228	3	194	5
D8012-1-19	88	165	0.54	0.0513	0.0030	0.2523	0.0146	0.0362	0.0006	0.0106	0.0003	254	131	228	12	229	3	214	6
D8012-1-20	100	190	0.52	0.0518	0.0029	0.2599	0.0139	0.0367	0.0005	0.0110	0.0003	276	128	235	11	232	3	222	6

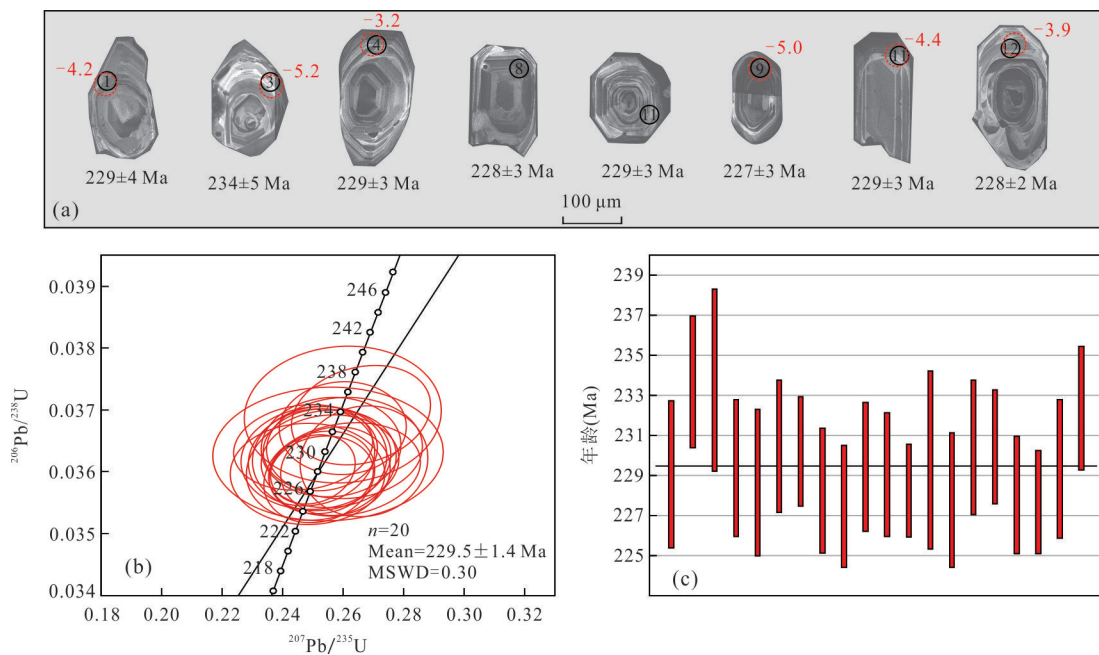


图3 石英闪长岩样品D8012-1典型锆石CL图(a)及U-Pb定年结果(b,c)

Fig.3 Cathodoluminescence images (a) and zircon U-Pb concordia diagrams (b, c) for zircons of quartz diorite sample (D8012-1). 图a中白色圆圈和红色圆圈分别代表U-Pb年代学、Hf同位素测试激光剥蚀点位, 对应黑色年龄和红色数字分别代表锆石 $^{206}\text{Pb}/^{238}\text{U}$ 表面年龄和 $\epsilon_{\text{Hf}}(\tau)$ 值; 圈中数字为分析点号, 编号同表1

表2 巴隆石英闪长岩主量元素(%)、微量元素和稀土元素(10^{-6})分析结果Table 2 Major elements (%), trace and REE elements (10^{-6}) data of the quartz diorite from Balong region

样品	BLWG-1	BLWG-2	BLWG-3	BLWG-4	BLWG-5	BLWG-6
	N 35.96°	N 35.96°	N 35.95°	N 35.95°	N 35.95°	N 35.95°
	E 97.38°	E 97.38°	E 97.35°	E 97.35°	E 97.38°	E 97.38°
SiO ₂	61.83	61.71	59.86	61.44	61.51	61.36
TiO ₂	0.62	0.71	0.76	0.70	0.67	0.68
Al ₂ O ₃	16.86	16.38	17.03	16.56	16.90	16.60
Fe ₂ O ₃ ^T	4.88	5.46	5.96	5.66	5.34	5.46
MnO	0.08	0.09	0.09	0.09	0.08	0.09
MgO	2.60	3.02	3.13	2.87	2.75	2.77
CaO	4.96	4.95	5.77	5.26	5.42	5.33
Na ₂ O	3.55	3.39	3.48	3.38	3.39	3.40
K ₂ O	2.85	2.68	2.50	2.71	2.64	2.72
P ₂ O ₅	0.14	0.16	0.18	0.16	0.16	0.16
LOI	0.94	0.72	0.69	0.70	0.96	0.57
Total	99.31	99.27	99.45	99.53	99.82	99.14
Na ₂ O/K ₂ O	1.25	1.26	1.39	1.25	1.28	1.25
Na ₂ O+K ₂ O	6.40	6.07	5.98	6.09	6.03	6.12
σ	2.18	1.97	2.12	2.01	1.96	2.04
A/CNK	0.94	0.94	0.90	0.92	0.92	0.91
A/NK	1.89	1.93	2.02	1.95	2.00	1.94
Mg [#]	51.3	52.3	51.0	50.1	50.5	50.1
Li	23.50	22.80	23.20	22.20	20.70	20.00
Be	1.85	1.52	1.74	1.65	1.77	1.99

续表2

样品	BLWG-1	BLWG-2	BLWG-3	BLWG-4	BLWG-5	BLWG-6
	N 35.96°	N 35.96°	N 35.95°	N 35.95°	N 35.95°	N 35.95°
	E 97.38°	E 97.38°	E 97.35°	E 97.35°	E 97.38°	E 97.38°
Sc	10.10	11.40	12.40	11.70	10.90	11.00
V	102.00	133.00	139.00	94.00	111.00	131.00
Cr	21.00	23.00	25.00	22.00	20.00	21.00
Co	90.30	103.00	104.00	68.50	80.00	91.80
Ni	57.40	62.50	63.70	44.50	50.30	55.90
Cu	15.70	9.30	19.20	9.20	30.10	10.20
Ga	19.15	19.30	20.50	19.40	19.40	19.80
Rb	116.00	111.50	100.50	104.50	97.90	111.00
Ba	644.00	582.00	608.00	649.00	586.00	552.00
Sr	572.00	474.00	509.00	609.00	518.00	504.00
Y	14.00	13.80	15.30	15.50	13.40	15.60
Zr	142.00	143.00	195.00	167.00	167.00	196.00
Nb	9.70	9.50	9.60	9.40	9.80	9.60
Sn	2.00	2.00	2.00	2.00	2.00	2.00
Cs	7.23	7.37	5.08	5.05	4.63	6.85
La	31.40	28.40	27.60	34.80	29.70	31.80
Ce	47.50	47.20	48.30	47.20	42.50	44.20
Pr	6.20	5.85	6.04	7.55	6.00	6.73
Nd	21.70	21.10	22.50	28.40	21.60	24.20
Sm	4.18	3.99	4.29	5.21	4.10	4.74
Eu	1.00	0.98	1.06	1.11	1.02	1.00
Gd	3.32	3.24	3.44	4.11	3.28	3.69
Tb	0.48	0.47	0.50	0.58	0.48	0.54
Dy	2.84	2.74	2.93	3.43	2.84	3.22
Ho	0.57	0.53	0.57	0.66	0.58	0.63
Er	1.57	1.48	1.63	1.90	1.50	1.70
Tm	0.24	0.22	0.24	0.35	0.23	0.26
Yb	1.47	1.34	1.48	1.75	1.44	1.71
Lu	0.23	0.22	0.22	0.32	0.22	0.25
Hf	4.00	3.80	4.90	4.70	4.30	5.20
Ta	1.52	1.60	1.44	1.22	1.43	1.64
Pb	17.30	15.60	17.50	27.40	16.90	17.50
Th	14.65	12.95	10.05	18.60	12.05	17.05
U	4.32	2.06	1.99	2.04	2.38	2.31
ΣREE	122.70	117.76	120.80	137.37	115.49	124.67
LREE	111.98	107.52	109.79	124.27	104.92	112.67
HREE	10.72	10.24	11.01	13.10	10.57	12.00
LREE/HREE	10.45	10.50	9.97	9.49	9.93	9.39
(La/Yb) _N	15.32	15.20	13.38	14.26	14.79	13.34
δEu	0.79	0.81	0.82	0.71	0.82	0.70
Sr/Y	40.86	34.35	33.27	39.29	38.66	32.31

注:A/CNK=Al₂O₃/(CaO+Na₂O+K₂O)摩尔比;A/NK=Al₂O₃/(Na₂O+K₂O)摩尔比;Mg[#]=100×molar MgO/(MgO+FeO);σ=(K₂O+Na₂O)²/(SiO₂-43);δEu={(Eu/0.058)/[(Sm/0.153)+(Gd/0.2055)]/2}.

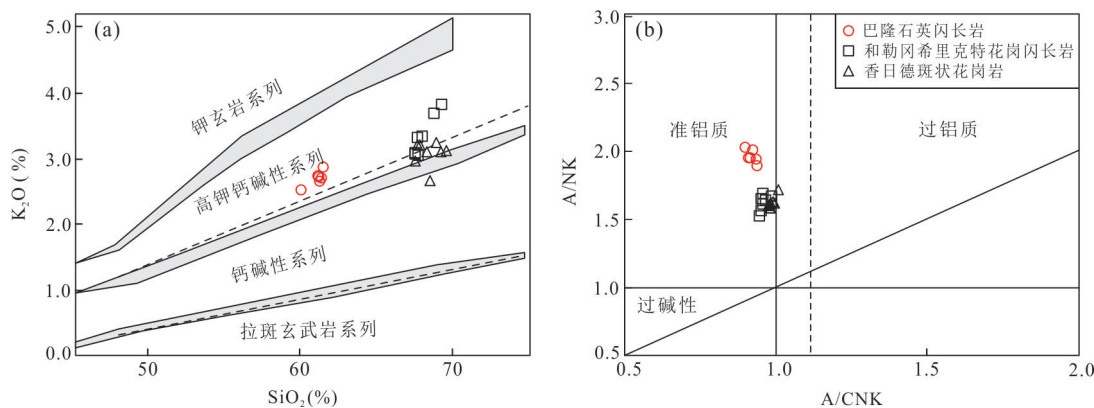
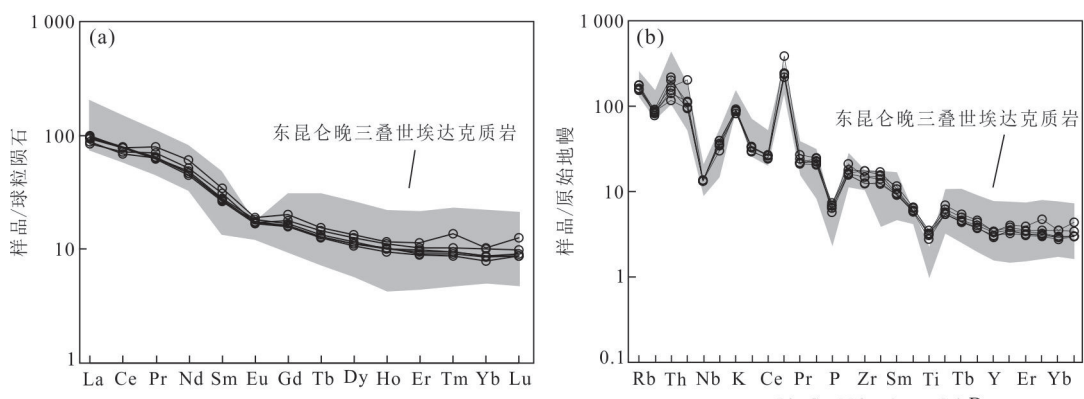
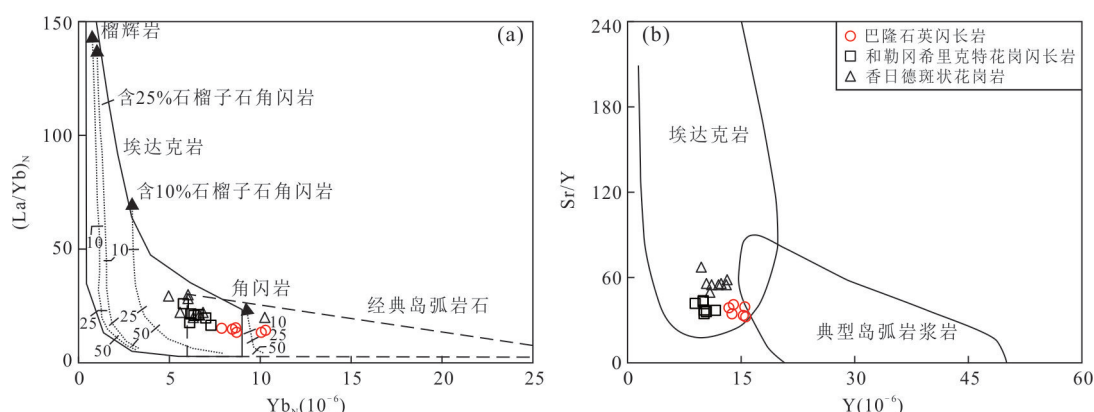
图4 巴隆石英闪长岩 $\text{SiO}_2-\text{K}_2\text{O}$ 图解(a)和 $\text{A}/\text{CNK}-\text{A}/\text{NK}$ 图解(b)Fig.4 $\text{K}_2\text{O}-\text{SiO}_2$ (a) and $\text{A}/\text{CNK}-\text{A}/\text{NK}$ (b) diagrams for the quartz diorite from Balong region图a底图据 Collins *et al.* (1982), 图b底图据 Maniar and Piccoli (1989). 数据来源: 和勒冈希里克特花岗闪长岩据陈国超等(2013b), 香日德斑状花岗岩据 Xiong *et al.* (2014)

图5 巴隆石英闪长岩稀土元素球粒陨石标准化配分图(a)和微量元素原始地幔标准化蛛网图(b)

Fig.5 Chondrite-normalized REE patterns (a) and primitive mantle-normalized trace element patterns (b) for the quartz diorite from Balong region

球粒陨石及原始地幔标准化数据引自 Sun and McDonough (1989); 东昆仑晚三叠世埃达克岩数据引自陈国超等(2013b), Xiong *et al.* (2014)图6 巴隆石英闪长岩 $\text{Yb}_N-(\text{La}/\text{Yb})_N$ 图解(a)和 $\text{Y}-\text{Sr}/\text{Y}$ 图解(b)Fig.6 $\text{Yb}_N-(\text{La}/\text{Yb})_N$ diagram (a) and $\text{Y}-\text{Sr}/\text{Y}$ diagram (b) for the quartz diorite from Balong region

图a、b底图据 Defant and Drummond (1990); 数据来源同图3, 图中带短线的虚线为部分熔融曲线

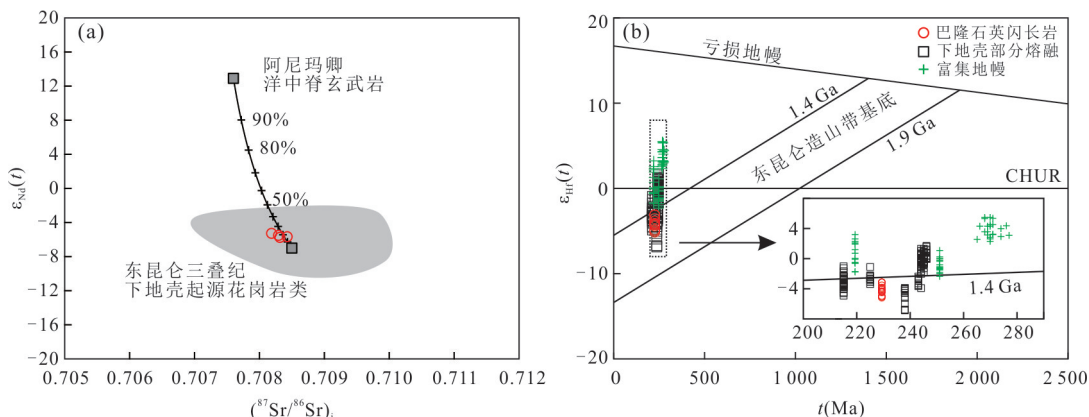
图 7 巴隆石英闪长岩($^{87}\text{Sr}/^{86}\text{Sr}$)— $\epsilon_{\text{Nd}}(t)$ 图解(a)和锆石 Hf 同位素图解(b)

Fig.7 ($^{87}\text{Sr}/^{86}\text{Sr}$)— $\epsilon_{\text{Nd}}(t)$ diagram (a) and Hf isotopic compositions of zircons (b) for the quartz diorite from Balong region. 图 a 阿尼玛卿洋中脊玄武岩数据来自郭安林等(2007), 东昆仑三叠纪下地壳起源花岗岩数据来自刘成东等(2003)、张宏飞等(2006)、Xiong et al. (2012)、Ding et al. (2014)、Li et al. (2015)、Chen et al. (2017); 图 b 底图据 Xiong et al. (2016), Hf 同位素下地壳部分熔融数据来自东昆仑五龙沟花岗岩、闪长岩(Ding et al. 2014)、香日德石英闪长岩、钾长花岗岩、斑状花岗岩(Xiong et al. 2014)、洪水河石英闪长岩、花岗闪长岩(Song et al., 2020), 富集地幔数据来自东昆仑白日其利辉长岩(熊富浩等, 2011)、阿克楚克塞辉长岩(杨锡铭等, 2018)、希望沟辉长岩(张志青等, 2019)

表 3 巴隆石英闪长岩全岩 Sm-Nd 同位素分析结果

Table 3 Sm-Nd isotopic compositions of the quartz diorite from Balong region

样品号	$^{87}\text{Rb}/^{86}\text{Sr}$	$^{87}\text{Sr}/^{86}\text{Sr}$	$\pm 1\sigma$	$(^{87}\text{Sr}/^{86}\text{Sr})_i$	$^{147}\text{Sm}/^{144}\text{Nd}$	$^{143}\text{Nd}/^{144}\text{Nd}$	$\pm 2\sigma$	$\epsilon_{\text{Nd}}(t)$	t_{DM1} (Ma)	t_{DM2} (Ma)
BLWG-1	0.639 4	0.710 52	0.000 03	0.708 428	0.116 4	0.512 227	0.000 004	-5.66	1 447	1 464
BLWG-2	0.747 0	0.710 63	0.000 04	0.708 186	0.114 3	0.512 244	0.000 003	-5.27	1 390	1 432
BLWG-3	0.594 8	0.710 24	0.000 02	0.708 294	0.115 3	0.512 233	0.000 003	-5.51	1 421	1 452
BLWG-5	0.606 7	0.710 30	0.000 02	0.708 315	0.114 7	0.512 220	0.000 004	-5.75	1 433	1 471

注: 计算采用 $(^{87}\text{Rb}/^{86}\text{Sr})_{\text{CHUR}}=0.082\ 7$; $(^{87}\text{Sr}/^{86}\text{Sr})_{\text{CHUR}}=0.704\ 5$; $\epsilon_{\text{Nd}}(t)$ 值计算采用 $(^{147}\text{Sm}/^{144}\text{Nd})_{\text{CHUR}}=0.196\ 7$; $(^{143}\text{Nd}/^{144}\text{Nd})_{\text{CHUR}}=0.512\ 638$; t 代表成岩年龄(230 Ma), 同位素亏损地幔模式年龄(t_{DM2})计算中采用 $(^{147}\text{Sm}/^{144}\text{Nd})_{\text{DM}}=0.213\ 6$; $(^{143}\text{Nd}/^{144}\text{Nd})_{\text{DM}}=0.513\ 1$ (Liew and Hofmann, 1988).

准化配分图解呈轻稀土元素富集, 重稀土元素相对亏损的右倾配分模式(图 5). 样品 $(\text{La}/\text{Yb})_N=13.34\sim 15.32$, 并具有 Eu 负异常(0.70~0.82). 微量元素方面, 样品具富集大离子亲石元素 Rb、Th、U 和 K, 显著亏损高场强元素 Nb、P 和 Ti.

上述主微量元素测试结果表明, 巴隆地区晚三叠世石英闪长岩与埃达克质岩地球化学特征相似. 埃达克质岩具有以下地球化学特征: $\text{SiO}_2 \geq 56\%$, $\text{Al}_2\text{O}_3 \geq 15\%$, $\text{Na}_2\text{O} > \text{K}_2\text{O}$, $\text{Sr} > 300 \times 10^{-6}$, $\text{Y} < 18 \times 10^{-6}$, $\text{Sr}/\text{Y} > 20$, $\text{Yb} < 1.9 \times 10^{-6}$, $\text{La}/\text{Yb} > 20$ (Martin, 1999; Castillo, 2006, 2012). 巴隆地区晚三叠世石英闪长岩 SiO_2 、 Al_2O_3 含量符合定义, 并且 $\text{K}_2\text{O}/\text{Na}_2\text{O}$ 为 0.71~0.80, 具有富钠特征, MgO 含量为 2.60%~3.13%, Sr 含量为 $474 \times 10^{-6} \sim 609 \times 10^{-6}$, Y 含量为 $13.40 \times 10^{-6} \sim 15.60 \times 10^{-6}$, La 含量为 $27.60 \times 10^{-6} \sim 37.80 \times 10^{-6}$, Yb 含量为 $1.34 \times 10^{-6} \sim 1.75 \times 10^{-6}$,

Sr/Y 为 32.31~40.86, $(\text{La}/\text{Yb})_N$ 为 13.37~15.35, 并具有 Eu 负异常(0.70~0.82). 主量、微量元素图解显示, 巴隆石英闪长岩与区域上典型的埃达克质岩(香日德斑状花岗岩、和勒岗希里克特花岗闪长岩)整体特征与保持一致(图 4、5). 在 $\text{Yb}_N-(\text{La}/\text{Yb})_N$ 图解和 $\text{Y}-\text{Sr}/\text{Y}$ 图解(图 6)中, 样品位置埃达克岩范围基本一致, 并与区域上同时代和勒岗希里克特花岗闪长岩和香日德斑状花岗岩相似. 因此, 本文判断巴隆石英闪长岩为埃达克质岩.

3.3 Sr-Nd-Hf 同位素

4 件石英闪长岩样品的 Sr-Nd 同位素测试结果列于表 3. 所有同位素参数计算所采用的年龄 $t=230$ Ma. 样品 $^{87}\text{Sr}/^{86}\text{Sr}$ 为 0.710 24~0.710 63, $^{143}\text{Nd}/^{144}\text{Nd}$ 为 0.512 220~0.512 244, $\epsilon_{\text{Nd}}(t)$ 为 -5.75~-5.27. 所有样品具有相似的模式年龄, 单阶段模式年龄 t_{DM} 为 1 390~1 447 Ma, 二阶段模

表4 巴隆石英闪长岩(D8012-1)锆石Hf同位素分析结果
Table 4 Hf isotopic data of the Balong quartz diorite sample (D8012-1)

测试点号	$^{176}\text{Hf}/^{177}\text{Hf}$	1σ	$^{176}\text{Lu}/^{177}\text{Hf}$	1σ	$^{176}\text{Yb}/^{177}\text{Hf}$	1σ	年龄 (Ma)	$\epsilon_{\text{Hf}}(0)$	1σ	$\epsilon_{\text{Hf}}(t)$	1σ	t_{DM1} (Ma)	t_{DM2} (Ma)	$f_{\text{Lu/Hf}}$
D8012-1-1	0.282 512	0.000 017	0.000 539	0.000 008	0.014 952	0.000 199	229	-9.2	0.8	-4.2	0.8	1 033	1 365	-0.98
D8012-1-2	0.282 506	0.000 018	0.000 829	0.000 014	0.022 396	0.000 363	234	-9.4	0.8	-4.4	0.8	1 050	1 377	-0.98
D8012-1-3	0.282 483	0.000 020	0.000 599	0.000 006	0.016 486	0.000 208	234	-10.2	0.9	-5.2	0.9	1 075	1 420	-0.98
D8012-1-4	0.282 541	0.000 016	0.000 527	0.000 008	0.014 571	0.000 186	229	-8.2	0.8	-3.2	0.8	993	1 308	-0.98
D8012-1-6	0.282 489	0.000 019	0.000 755	0.000 014	0.020 371	0.000 298	230	-10.0	0.8	-5.1	0.8	1 073	1 413	-0.98
D8012-1-8	0.282 504	0.000 021	0.000 536	0.000 006	0.015 361	0.000 141	228	-9.5	0.9	-4.5	0.9	1 044	1 381	-0.98
D8012-1-9	0.282 493	0.000 019	0.000 757	0.000 025	0.020 783	0.000 720	227	-9.9	0.8	-5.0	0.9	1 067	1 406	-0.98
D8012-1-10	0.282 508	0.000 018	0.000 439	0.000 008	0.012 201	0.000 201	229	-9.3	0.8	-4.4	0.8	1 036	1 372	-0.99
D8012-1-11	0.282 507	0.000 019	0.000 428	0.000 004	0.012 229	0.000 167	229	-9.4	0.9	-4.4	0.9	1 038	1 375	-0.99
D8012-1-12	0.282 523	0.000 018	0.000 451	0.000 007	0.011 986	0.000 163	228	-8.8	0.8	-3.9	0.8	1 016	1 343	-0.99
D8012-1-14	0.282 544	0.000 019	0.000 638	0.000 014	0.018 573	0.000 359	228	-8.1	0.8	-3.2	0.9	992	1 305	-0.98
D8012-1-15	0.282 518	0.000 017	0.000 728	0.000 010	0.021 449	0.000 197	230	-9.0	0.8	-4.0	0.8	1 031	1 355	-0.98
D8012-1-16	0.282 513	0.000 018	0.000 626	0.000 017	0.018 404	0.000 473	230	-9.2	0.8	-4.2	0.8	1 035	1 365	-0.98
D8012-1-17	0.282 541	0.000 021	0.000 676	0.000 010	0.019 806	0.000 222	228	-8.2	0.9	-3.2	0.9	997	1 310	-0.98
D8012-1-18	0.282 543	0.000 023	0.000 787	0.000 017	0.023 570	0.000 476	228	-8.1	1.0	-3.2	1.0	998	1 307	-0.98
D8012-1-20	0.282 527	0.000 018	0.000 413	0.000 001	0.011 755	0.000 094	232	-8.7	0.8	-3.6	0.8	1 010	1 335	-0.99

注:分析点保留U-Pb定点的分析点号: $\epsilon_{\text{Hf}}(0)=10 000 \times [(^{176}\text{Hf}/^{177}\text{Hf})_S/(^{176}\text{Hf}/^{177}\text{Hf})_{\text{CHUR},0}-1]$; $f_{\text{Lu/Hf}}=(^{176}\text{Lu}/^{177}\text{Hf})_S/(^{176}\text{Lu}/^{177}\text{Hf})_{\text{CHUR}}-1$;
 $\epsilon_{\text{Hf}}(t)=10 000 \times \{[(^{176}\text{Hf}/^{177}\text{Hf})_S-(^{176}\text{Lu}/^{177}\text{Hf})_S \times (e^{\lambda t}-1)]/[(^{176}\text{Hf}/^{177}\text{Hf})_{\text{CHUR},0}-(^{176}\text{Lu}/^{177}\text{Hf})_{\text{CHUR}} \times (e^{\lambda t}-1)]-1\}$; $t_{\text{DM}}=1/\lambda \times \ln\{1+[(^{176}\text{Hf}/^{177}\text{Hf})_S-(^{176}\text{Hf}/^{177}\text{Hf})_{\text{DM}}]/[(^{176}\text{Lu}/^{177}\text{Hf})_S-(^{176}\text{Lu}/^{177}\text{Hf})_{\text{DM}}]\}$; $t_{\text{DM2}}=t_{\text{DM}}\text{Hf}-(t_{\text{DM}}\text{Hf}-t) \times [(f_{\text{CC}}-f_{\text{S}})/(f_{\text{CC}}-f_{\text{DM}})]$; $(^{176}\text{Lu}/^{177}\text{Hf})_{\text{CHUR}}=0.0332$, $(^{176}\text{Hf}/^{177}\text{Hf})_{\text{CHUR},0}=0.282 772$ (Blichert-Toft *et al.*, 1997), $(^{176}\text{Lu}/^{177}\text{Hf})_{\text{DM}}=0.0384$ (Griffin *et al.*, 2000), $(^{176}\text{Hf}/^{177}\text{Hf})_{\text{DM}}=0.28325$ (Nowell *et al.*, 1998); $(^{176}\text{Lu}/^{177}\text{Hf})_{\text{CC}}=0.015$, $f_{\text{CC}}=-0.548$, $f_{\text{DM}}=0.16$ (Griffin *et al.*, 2000), $\lambda=1.867 \times 10^{-11} \text{ a}^{-1}$ (Söderlund *et al.*, 2004).

式年龄 t_{DM2} 为 1 432~1 471 Ma(图 7).

锆石Hf同位素分析结果见表4.16个样品点的 $^{176}\text{Yb}/^{177}\text{Hf}$ 为0.011 755~0.023 570, $^{176}\text{Lu}/^{177}\text{Hf}$ 为0.000 413~0.000 829, $^{176}\text{Hf}/^{177}\text{Hf}$ 为0.282 483~0.282 544. 以对应的锆石U-Pb年龄计算出锆石 $\epsilon_{\text{Hf}}(t)=-5.2\sim-3.2$, 二阶段Hf模式年龄 $t_{\text{DM2}}(\text{Hf})=1 305\sim1 420$ Ma.

4 讨论

4.1 岩石成因

如3.2所述,本文判断巴隆石英闪长岩为埃达克质岩. 关于埃达克质岩的成因,前人提出其可以来源于多种源区,形成于多种过程,主要的成因模式包括:(1)俯冲板片的部分熔融(Rapp *et al.*, 1999);(2)玄武质岩浆的分离结晶(Castillo *et al.*, 1999);(3)拆沉下地壳的部分熔融(Xu *et al.*, 2002; Gao *et al.*, 2004);(4)增厚的玄武质下地壳的部分熔融(Chung *et al.*, 2003).

巴隆石英闪长岩体 $\text{Na}_2\text{O}=3.38\%\sim3.55\%$, 平均3.43%; $\text{Na}_2\text{O}/\text{K}_2\text{O}=1.25\%\sim1.39\%$, 平均1.28%;

岩体的初始 $^{87}\text{Sr}/^{86}\text{Sr}$ 值为0.710 24~0.710 63,与典型的俯冲板片熔融形成的埃达克质岩石的特征($\text{Na}_2\text{O}/\text{K}_2\text{O}>12$ 、Sr同位素初始值<0.704 5以及 $\epsilon_{\text{Hf}}(t)>6$)明显不同(Defant and Drummond, 1990; 张旗等, 2009),暗示与俯冲板片部分熔融有关的成因模式并不适用于巴隆石英闪长岩.

玄武质岩浆分离结晶形成埃达克质岩石的过程中会形成基性-中性-酸性岩石系列(Castillo *et al.*, 1999),并且 Al_2O_3 的含量极高(可达18%; Macpherson *et al.*, 2006). 研究区内未发现与研究对象同时代的基性侵入岩,样品的 Al_2O_3 含量也明显低于上述数值. 同时在通常情况下,高压条件下的结晶分异过程涉及石榴石,导致岩石中HREE和Y的含量降低,会导致 Dy/Yb 和 Sr/Y 与 SiO_2 呈正相关,低压条件下的结晶分异过程涉及橄榄石、辉石、斜长石与角闪石,导致 MgO 、Cr、Ni等元素与 SiO_2 呈负相关(Castillo *et al.*, 1999),巴隆石英闪长岩未表现出上述相关特征. 此外, $\text{Zr}-\text{Zr}/\text{Nb}$ 图解与 $\text{FeO}^\text{T}-\text{MgO}$ 图解(图8)中,样品均偏离结晶分离趋势线,表明分离结晶作用不是岩体形成的主导方式. 因此,巴隆石英闪长岩不太可能形成于分离结晶形

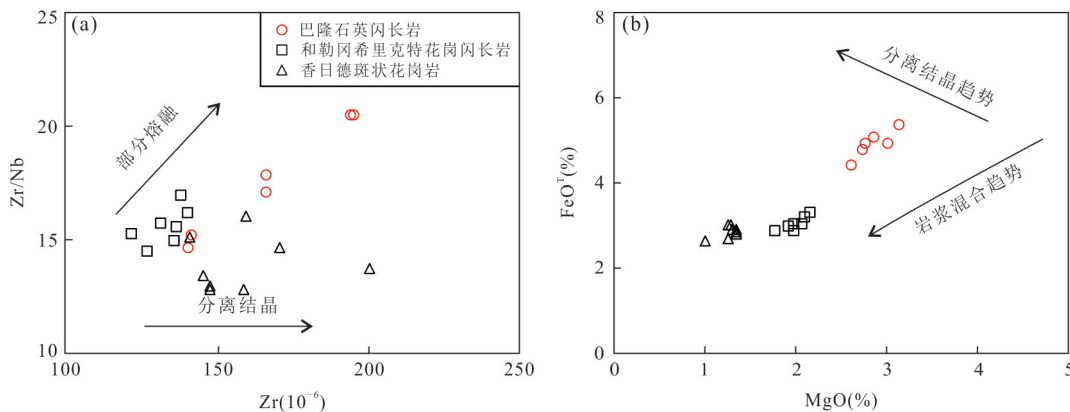


图 8 巴隆石英闪长岩 Zr—Zr/Nb 图解和 MgO—FeOT 图解

Fig.8 Zr—Zr/Nb diagram (a) and MgO—FeOT diagram (b) for the quartz diorite from Balong region
底图据 Zorpi *et al.*(1991); 数据来源同图 3

成过程。

通常情况下,由拆沉下地壳部分熔融形成的埃达克质岩,在岩浆上涌过程中会与地幔橄榄岩反应,产生MgO含量大于3%、Mg#大于50并且Cr、Ni含量较高的埃达克质熔体(Smithies, 2000; Prouteau *et al.*, 2001)。同时,与拆沉下地壳部分熔融形成的埃达克质岩的锆石中往往存在大量继承锆石(高山等, 2009)。然而巴隆石英闪长岩显示低的Cr、Ni含量,且未出现明显继承锆石,指示拆沉下地壳熔融模型无法解释巴隆石英闪长岩的成因模式。

巴隆石英闪长岩样品具有负的 $\epsilon_{\text{Hf}}(\tau)$ (−5.2~−3.2),与东昆仑地区下地壳熔融的岩体较为相似;较老的Hf(1 305~1 420 Ma)和Nd(1 432~1 471 Ma)二阶段模式年龄亦表明其源区具有中元古代地壳物质。图7a中,样品落于MORB下地壳的演化线上,并与东昆仑地区下地壳部分熔融形成的岩浆岩具有相似的Sr-Nd同位素组成,表明岩石起源于下地壳的部分熔融。此外,在图9a中,样品落入了增厚下地壳熔融形成的埃达克岩区域,指示岩石成因可能与加厚下地壳部分熔融密切相关。根据Hu *et al.*(2017)提出的碰撞造山背景下全岩Sr/Y与地壳厚度的关系公式:Sr/Y=(1.49±0.15)H−(42.03±6.28)(该式适用条件是SiO₂含量为55%~72%且MgO含量为0.5%~6.0%),本文计算出东昆仑地区在~230 Ma时地壳厚度为49~70 km,明显高于240~260 Ma时地壳厚度估算结果(图9b),说明巴隆石英闪长岩形成时,地壳处于增厚状态,佐证了加厚下地壳与成岩的密切联系。

巴隆石英闪长岩具有高Sr/Y和La/Yb、低Y和HREE含量的特征,并具有相对较低的Al₂O₃/

(FeO^T+MgO+TiO₂)、(Na₂O+K₂O)/(FeO^T+MgO+TiO₂),与实验岩石学论证的下地壳角闪岩类熔融产生的熔体成分相似(图9c、9d),指示岩浆可能来源于基性下地壳的部分熔融。前人研究表明,压力大于1.5 GPa(深度大于50 km)时,石榴子石和角闪石在残留相中占主导地位而斜长石消失(Sen and Dunn, 1994)。同时,样品微量元素具有较高的Sr/Y、(La/Yb)_N、低Y和HREE含量,指示在熔融过程中石榴子石作为主要残留矿物导致重稀土明显分异(Rapp and Watson, 1995)。相对平坦的HREE配分模式表明在岩浆形成中角闪石相较石榴子石占主导作用(Moyen, 2009)。综上所述,巴隆石英闪长岩可能来源于增厚的角闪质下地壳的部分熔融,源区残留石榴子石等矿物。

考虑到地壳加厚过程中压力增加导致温度无法达到熔融的固相线(罗照华等, 2007),地壳岩石发生部分熔融通常需要外来异常的加热作用。一般情况下,幔源岩浆底侵下地壳可以满足这一需求。巴隆石英闪长岩的岩相学、岩石地球化学证据支持上述过程,并表明幔源岩浆的底侵不仅为成岩提供了热源,同时还提供了一部分物质来源。证据如下:(1)巴隆石英闪长岩具有镁铁质包体。镁铁质包体具有典型的岩浆岩矿物组合和结构构造,未见石榴子石、堇青石等典型富铝矿物,排除壳源残留体的可能;包体形态多为椭圆状,与捕虏体在形态上具有较大差别(Vernon, 1984);包体粒度明显小于寄主岩体,该特征与同源岩浆早期形成的析离体、堆晶体明显不同;由此推测,包体应为岩浆混合成因。(2)显微镜下可见斜长石具有环带结构(图2f),并发育有针状磷灰石,表明岩体可能经历了多期次的岩

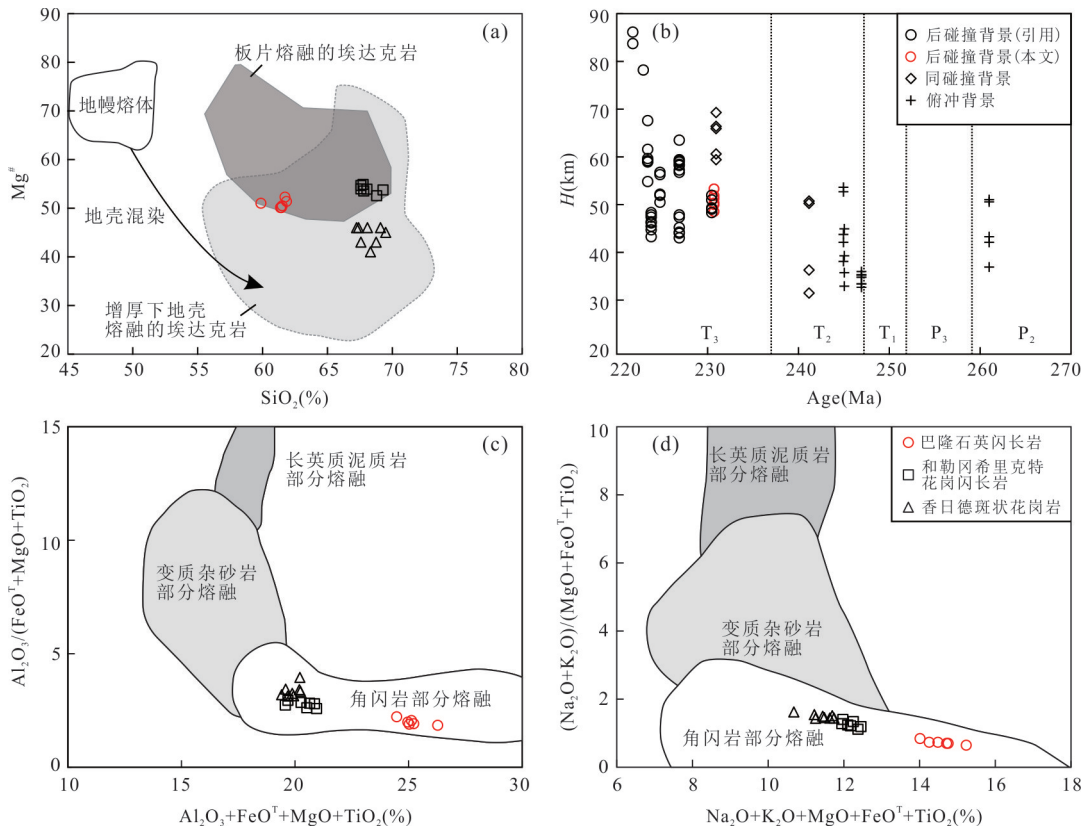


图9 巴隆石英闪长岩 $\text{SiO}_2-\text{Mg}^{\#}$ 图解(a)、 Sr/Y 估算地壳厚度与年龄关系图(b)、 $(\text{Al}_2\text{O}_3+\text{FeO}^{\text{T}}+\text{MgO}+\text{TiO}_2)-\text{Al}_2\text{O}_3/(\text{FeO}^{\text{T}}+\text{MgO}+\text{TiO}_2)$ 图解(c)及 $(\text{Na}_2\text{O}+\text{K}_2\text{O}+\text{MgO}+\text{FeO}^{\text{T}}+\text{TiO}_2)-(\text{Na}_2\text{O}+\text{K}_2\text{O})/(\text{FeO}^{\text{T}}+\text{MgO}+\text{TiO}_2)$ 图解(d)

Fig.9 $\text{SiO}_2-\text{Mg}^{\#}$ diagram (a), age-crustal thickness estimated from Sr/Y diagram (b), $(\text{Al}_2\text{O}_3+\text{FeO}^{\text{T}}+\text{MgO}+\text{TiO}_2)-\text{Al}_2\text{O}_3/(\text{FeO}^{\text{T}}+\text{MgO}+\text{TiO}_2)$ diagram (c) and $(\text{Na}_2\text{O}+\text{K}_2\text{O}+\text{MgO}+\text{FeO}^{\text{T}}+\text{TiO}_2)-(\text{Na}_2\text{O}+\text{K}_2\text{O})/(\text{FeO}^{\text{T}}+\text{MgO}+\text{TiO}_2)$ diagram (d) for the quartz diorite from Balong region

图a底图据Hou *et al.* (2004),图c,d底图据Patino Douce(1999);图a,c,d数据来源同图3,图b后碰撞背景数据据陈国超等(2013b)、夏锐等(2014)、Xiong *et al.* (2014)、罗明非等(2014)、Li *et al.* (2015),同碰撞背景数据据Zhang *et al.* (2012)、国显正等(2016),俯冲背景数据据Xiong *et al.* (2012, 2014)、Ding *et al.* (2015)、Song *et al.* (2020)

浆演化。(3)图7a中,本文选取阿尼玛卿洋中脊玄武岩数据,将其校正为 $t=230$ Ma,作为地幔端元,代表该时期研究区深部可能存在的地幔源区,样品靠近与东昆仑同时代下地壳部分熔融产生的花岗岩类的演化线,代表源区有少量幔源物质的加入。(4)样品的 $\epsilon_{\text{Hf}}(t)$ 值变化于 $-5.2 \sim -3.2$ 之间,与下地壳源区的岩石有所不同(图7b),支持幔源物质对岩体的贡献。由此可见,巴隆石英闪长岩的形成更有可能是壳幔岩浆混合的结果。

岩浆混合作用包括岩浆化学混合和岩浆机械混合(王玉往等,2012)。巴隆石英闪长岩的镁铁质包体呈椭圆状分布于寄主岩中,说明包体与寄主岩浆曾塑性共存,且存在机械混合;而镜下斜长石的环带结构表明矿物形成过程中岩浆成分的变化,暗示存在化学混合。磷灰石等矿物的存在佐证了混合过程中温度较高的基性岩浆注入温度较低的偏酸性

岩浆的过程(张泽斌等,2019)。同时,上述岩石特征也表明岩浆混合尚处于较为初级的阶段。这合理解释了寄主岩石 Sr-Nd-Hf 同位素组成主要与下地壳起源的花岗岩保持一致的现象。

综上所述,巴隆石英闪长岩的形成与下地壳加厚状态下壳幔岩浆混合密切相关。玄武质岩浆底侵诱导加厚下地壳发生部分熔融形成大量高钾钙碱性埃达克质熔体,岩浆底侵过程中的少量的幔源玄武质熔体与下地壳埃达克质熔体发生岩浆混合作用,形成了巴隆石英闪长岩。

4.2 构造背景

东昆仑地区广泛发育的晚古生代—中生代岩浆岩与古特提斯洋的演化密切相关(莫宣学等,2007)。年代学研究表明,古特提斯洋俯冲开始时间不晚于 278 Ma(Chen *et al.*, 2001; 刘战庆等, 2011; Liu *et al.*, 2014)。上二叠统格曲组底部的黄绿色水

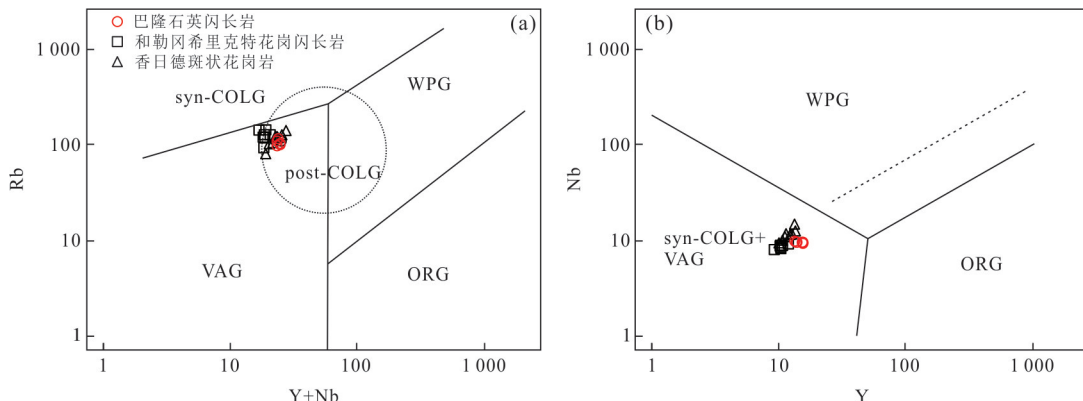


图 10 巴隆石英闪长岩构造环境判别图解

Fig.10 Tectonic discrimination diagrams for the quartz diorite from Balong region

Syn-COLG. 同碰撞花岗岩;WPG. 板内花岗岩;VAG. 火山弧花岗岩;ORG. 洋脊花岗岩;底图据 Pearce *et al.*(1984);数据来源同图 3

下磨拉石沉积组合被认为是古特提斯洋开始俯冲的同构造沉积响应(李瑞保,2012).目前对于古特提斯洋的闭合时间存在争议,认为闭合时间在晚二叠世(Huang *et al.*, 2014)、早一中三叠世(Xiong *et al.*, 2014; Chen *et al.*, 2017; Kong *et al.*, 2020)或是晚三叠世(Roger *et al.*, 2003; Ding *et al.*, 2014).

早一中三叠世东昆仑地区形成了大量与俯冲相关的弧岩浆岩(Xiong *et al.*, 2012, 2014),其中包括富含镁铁质包体的钙碱性 I型花岗岩(Xiong *et al.*, 2012; 李瑞保等, 2018; Li *et al.*, 2020)以及有限的辉长岩(Xiong *et al.*, 2014; Chen *et al.*, 2017; 赵旭等, 2018)和火山岩(吴芳等, 2010; Xiao *et al.*, 2015).这些岩石的形成多与俯冲流体交代地幔楔熔融并诱导下地壳熔融有关.同时,区域上早一中三叠世洪水川组具典型大陆斜坡深海相沉积特征,闹仓坚沟组具有弧前沉积盆地特征(闫臻等, 2008),可以说明该时期东昆仑地区处于俯冲的陆缘弧环境,古特提斯洋俯冲时间至少持续至中三叠世.

巴隆石英闪长岩形成于 230 Ma,如前文所述,该岩体为埃达克质岩,由加厚下地壳的部分熔融形成,在形成过程中还存在幔源物质的加入. 埃达克质岩是后碰撞拉伸环境的典型标志之一,在构造环境判别图中,石英闪长岩样品与同时期的香日德斑状花岗岩、和勒冈西里可特花岗闪长岩相似,均有后碰撞花岗岩的特征(图 10a, 10b).因此推测,巴隆石英闪长岩产于后碰撞的局部拉张环境,限定了在 230 Ma 时古特提斯洋已经闭合.

后碰撞的动力条件下,“俯冲洋壳板片断离”模式(陈国超等, 2018, 2019)可以较好解释幔源岩浆的上涌与底侵. 板片断离使软流圈物质上涌,诱发

地幔楔的减压熔融,产生镁铁质岩浆并底侵下地壳. 近年研究表明,东昆仑晚三叠世岩浆岩沿昆中断裂带分布,与板片断离作用产生的线状分布的岩浆岩较为一致;东昆仑地区与古特提斯洋俯冲相关的岩浆岩形成于晚二叠世—中三叠世,而与碰撞、后碰撞相关的岩浆岩多形成于晚三叠世,两者时间间隔约为 10 Ma,与板片断离模式较为符合;地球物理资料也证明了板片断离存在的可能,邓晋福等(1995)对格尔木—额济纳旗地学断面的研究表明,东昆仑—柴达木地区莫霍面之下存在厚度为 25~30 km 的基性榴辉岩上地幔岩石圈,其可能是由于板片断离而落入上地幔,使幔源岩浆底侵的产物. 因此可以初步推断,东昆仑地区晚三叠世的花岗岩浆作用可能是对碰撞后洋壳断离事件的响应.

5 结论

(1) 巴隆石英闪长岩锆石 LA-ICP-MS U-Pb 年龄为 229.5 Ma, 指示岩体侵位于晚三叠世.

(2) 岩石地球化学特征显示巴隆石英闪长岩具有埃达克质岩的特征,结合 Sr-Nd-Hf 同位素组成特征,岩体成因与增厚下地壳部分熔融形成的熔体和幔源岩浆混合作用有关.

(3) 巴隆石英闪长岩形成于古特提斯后碰撞伸展背景,是对碰撞后洋壳断离事件的响应.

致谢: 参加野外工作的还有王大钊博士、牛明伟硕士等,论文的撰写与修改得到了陈加杰博士、周红智博士、赵旭博士的帮助与支持,匿名审稿专家和编辑部老师对文章进行了认真的审阅,提出了建设性的意见,在此一并表示感谢!

References

- Blichert-Toft, J., Chauvel, C., Albarède, F., 1997. Separation of Hf and Lu for High-Precision Isotope Analysis of Rock Samples by Magnetic Sector-Multiple Collector ICP-MS. *Contributions to Mineralogy and Petrology*, 127(3): 248–260. <https://doi.org/10.1007/s004100050278>
- Castillo, P. R., 2006. An Overview of Adakite Petrogenesis. *Chinese Science Bulletin*, 51(3): 257–268. <https://doi.org/10.1007/s11434-006-0257-7>
- Castillo, P. R., 2012. Adakite Petrogenesis. *Lithos*, 134–135: 304–316. <https://doi.org/10.1016/j.lithos.2011.09.013>
- Castillo, P. R., Janney, P. E., Solidum, R. U., 1999. Petrology and Geochemistry of Camiguin Island, Southern Philippines: Insights to the Source of Adakites and Other Lavas in a Complex Arc Setting. *Contributions to Mineralogy and Petrology*, 134(1):33–51. <https://doi.org/10.1007/s004100050467>
- Chen, G. C., Pei, X. Z., Li, R. B., et al., 2013a. Zircon U-Pb Geochronology, Geochemical Characteristics and Geological Significance of Cocoe A'Long Quartz Diorites Body from the Hongshuichuan Area in East Kunlun. *Acta Geologica Sinica*, 87(2): 178–196(in Chinese with English abstract).
- Chen, G. C., Pei, X. Z., Li, R. B., et al., 2013b. Geochronology and Genesis of the Helegang Xilikete Granitic Plutons from the Southern Margin of the Eastern East Kunlun Orogenic Belt and Their Tectonic Significance. *Acta Geologica Sinica*, 87(10): 1525–1541(in Chinese with English abstract).
- Chen, G. C., Pei, X. Z., Li, R. B., et al., 2018. Age and Lithogenesis of Keri Syenogranite from Eastern Part of East Kunlun Orogenic Belt: Constraint on the Middle Triassic Tectonic Evolution of East Kunlun. *Acta Petrologica Sinica*, 34(3):567–585(in Chinese with English abstract).
- Chen, G. C., Pei, X. Z., Li, R. B., et al., 2019. Lithospheric Extension of the Post-Collision Stage of the Paleo-Tethys Oceanic System in the East Kunlun Orogenic Belt: Insights from Late Triassic Plutons. *Earth Science Frontiers*, 26(4):191–208(in Chinese with English abstract).
- Chen, J. J., Wei, J. H., Fu, L. B., et al., 2017. Multiple Sources of the Early Mesozoic Gouli Batholith, Eastern Kunlun Orogenic Belt, Northern Tibetan Plateau: Linking Continental Crustal Growth with Oceanic Subduction. *Lithos*, 292–293: 161–178. <https://doi.org/10.1016/j.lithos.2017.09.006>
- Chen, L., Sun, Y., Pei, X. Z., et al., 2001. Northernmost Paleo-Tethyan Oceanic Basin in Tibet: Geochronological Evidence from $^{40}\text{Ar}/^{39}\text{Ar}$ Age Dating of Dur'ngoi Ophiolite. *Chinese Science Bulletin*, 46(14): 1203–1205. <https://doi.org/10.1007/bf02900603>
- Chung, S. L., Liu, D. Y., Ji, J. Q., et al., 2003. Adakites from Continental Collision Zones: Melting of Thickened Lower Crust beneath Southern Tibet. *Geology*, 31(11):1021–1024. <https://doi.org/10.1130/g19796.1>
- Collins, W. J., Beams, S. D., White, A. J. R., et al., 1982. Nature and Origin of A-Type Granites with Particular Reference to Southeastern Australia. *Contributions to Mineralogy and Petrology*, 80(2): 189–200. <https://doi.org/10.1007/bf00374895>
- Defant, M. J., Drummond, M. S., 1990. Derivation of Some Modern Arc Magmas by Melting of Young Subducted Lithosphere. *Nature*, 347: 662–665. <https://doi.org/10.1038/347662a0>
- Deng, J. F., Wu, Z. X., Yang, J. J., et al., 1995. Crust-Mantle Petrological Structure and Deep Processes along the Golmud-Ejin Qi Geoscience Section. *Chinese Journal of Geophysics*, 38(Suppl. 2): 130–144(in Chinese with English abstract).
- Ding, Q. F., Jiang, S. Y., Sun, F. Y., 2014. Zircon U-Pb Geochronology, Geochemical and Sr-Nd-Hf Isotopic Compositions of the Triassic Granite and Diorite Dikes from the Wulonggou Mining Area in the Eastern Kunlun Orogen, NW China: Petrogenesis and Tectonic Implications. *Lithos*, 205: 266–283. <https://doi.org/10.1016/j.lithos.2014.07.015>
- Ding, Q. F., Liu, F., Yan, W., 2015. Zircon U-Pb Geochronology and Hf Isotopic Constraints on the Petrogenesis of Early Triassic Granites in the Wulonggou Area of the Eastern Kunlun Orogen, Northwest China. *International Geology Review*, 57(13): 1735–1754. <https://doi.org/10.1080/00206814.2015.1029541>
- Gao, S., Rudnick, R. L., Yuan, H. L., et al., 2004. Recycling Lower Continental Crust in the North China Craton. *Nature*, 432(7019): 892–897. <https://doi.org/10.1038/nature03162>
- Gao, S., Zhang, J. F., Xu, W. L., et al., 2009. Delamination and Destruction of the North China Craton. *Chinese Science Bulletin*, 54(14):1962–1973(in Chinese).
- Griffin, W. L., Belousova, E. A., Shee, S. R., et al., 2004. Archean Crustal Evolution in the Northern Yilgarn Craton: U-Pb and Hf-Isotope Evidence from Detrital Zircons. *Precambrian Research*, 131(3–4):231–282. <https://doi.org/10.1016/j.precamres.2003.12.011>
- Griffin, W. L., Pearson, N. J., Belousova, E., et al., 2000. The Hf Isotope Composition of Cratonic Mantle: LAM-MC-

- ICPMS Analysis of Zircon Megacrysts in Kimberlites. *Geochimica et Cosmochimica Acta*, 64(1): 133–147. [https://doi.org/10.1016/s0016-7037\(99\)00343-9](https://doi.org/10.1016/s0016-7037(99)00343-9)
- Guo, A.L., Zhang, G.W., Sun, Y.G., et al., 2007. Sr-Nd-Pb Isotopic Geochemistry of Late-Paleozoic Mafic Volcanic Rocks in the Surrounding Areas of the Gonghe Basin, Qinghai Province and Geological Implications. *Acta Petrologica Sinica*, 23(4):747—754(in Chinese with English abstract).
- Guo, X.Z., Jia, Q.Z., Li, Y.Z., et al., 2016. Zircon U-Pb Geochronology and Geochemical Characteristics of the Reshui Monzogranite in the Eastern Kunlun and Their Tectonic Significances. *Bulletin of Mineralogy, Petrology and Geochemistry*, 35(6): 1318—1328(in Chinese with English abstract).
- Hou, Z.Q., Gao, Y.F., Qu, X.M., et al., 2004. Origin of Adakitic Intrusives Generated during Mid-Miocene East-West Extension in Southern Tibet. *Earth and Planetary Science Letters*, 220(1–2): 139—155. [https://doi.org/10.1016/s0016-821x\(04\)00007-x](https://doi.org/10.1016/s0016-821x(04)00007-x)
- Hu, C.B., Li, M., Zha, X.F., et al., 2018. Genesis and Geological Significance of Late Paleozoic Mantle-Derived Magmatism in Qimantag, East Kunlun: A Case Study of Intrusion in Yingzhuagou. *Earth Science*, 43(12): 4334—4349 (in Chinese with English abstract).
- Hu, F.Y., Ducea, M.N., Liu, S.W., et al., 2017. Quantifying Crustal Thickness in Continental Collisional Belts: Global Perspective and a Geologic Application. *Scientific Reports*, 7: 7058 <https://doi.org/10.1038/s41598-017-07849-7>
- Hu, Y., Niu, Y.L., Li, J.Y., et al., 2016. Petrogenesis and Tectonic Significance of the Late Triassic Mafic Dikes and Felsic Volcanic Rocks in the East Kunlun Orogenic Belt, Northern Tibet Plateau. *Lithos*, 245: 205—222. <https://doi.org/10.1016/j.lithos.2015.05.004>
- Hu, Z.C., Liu, Y.S., Gao, S., et al., 2012. Improved In Situ Hf Isotope Ratio Analysis of Zircon Using Newly Designed X Skimmer Cone and Jet Sample Cone in Combination with the Addition of Nitrogen by Laser Ablation Multiple Collector ICP-MS. *Journal of Analytical Atomic Spectrometry*, 27(9): 1391—1399. <https://doi.org/10.1039/c2ja30078h>
- Huang, H., Niu, Y.L., Nowell, G., et al., 2014. Geochemical Constraints on the Petrogenesis of Granitoids in the East Kunlun Orogenic Belt, Northern Tibetan Plateau: Implications for Continental Crust Growth through Syn-Collisional Felsic Magmatism. *Chemical Geology*, 370: 1—18. <https://doi.org/10.1016/j.chemgeo.2014.01.010>
- Kong, J.J., Niu, Y.L., Hu, Y., et al., 2020. Petrogenesis of the Triassic Granitoids from the East Kunlun Orogenic Belt, NW China: Implications for Continental Crust Growth from Syn-Collisional to Post-Collisional Setting. *Lithos*, 364—365: 105513. <https://doi.org/10.1016/j.lithos.2020.105513>
- Li, B.L., Zhi, Y.B., Zhang, L., et al., 2015. U-Pb Dating, Geochemistry, and Sr-Nd Isotopic Composition of a Granodiorite Porphyry from the Jiadanggen Cu-(Mo) Deposit in the Eastern Kunlun Metallogenic Belt, Qinghai Province, China. *Ore Geology Reviews*, 67:1—10. <https://doi.org/10.1016/j.oregeorev.2014.11.008>
- Li, R.B., 2012. Research on the Late Paleozoic-Early Mesozoic Orogeny in East Kunlun Orogen (Dissertation). Chang'an University, Xi'an (in Chinese with English abstract).
- Li, R.B., Pei, X.Z., Li, Z.C., et al., 2018. Paleo-Tethys Ocean Subduction in Eastern Section of East Kunlun Orogen: Evidence from the Geochronology and Geochemistry of the Wutuo Pluton. *Acta Petrologica Sinica*, 34(11): 3399—3421(in Chinese with English abstract).
- Li, W.Y., Zhang, Z.W., Gao, Y.B., et al., 2011. Important Metallogenic Events and Tectonic Response of Qinling, Qilian and Kunlun Orogenic Belts. *Geology in China*, 38 (5):1135—1149(in Chinese with English abstract).
- Li, Y.J., Wei, J.H., Santosh, M., et al., 2020. Anisian Granodiorites and Mafic Microgranular Enclaves in the Eastern Kunlun Orogen, NW China: Insights into Closure of the Eastern Paleo-Tethys. *Geological Journal*, 55(9):6487—6507. <https://doi.org/10.1002/gj.3814>
- Liew, T.C., Hofmann, A.W., 1988. Precambrian Crustal Components, Plutonic Associations, Plate Environment of the Hercynian Fold Belt of Central Europe: Indications from Nd and Sr Isotopic Study. *Contributions to Mineralogy and Petrology*, 98(2): 129—138. <https://doi.org/10.1007/bf00402106>
- Liu, B., Ma, C.Q., Zhang, J.Y., et al., 2014. ^{40}Ar - ^{39}Ar Age and Geochemistry of Subduction-Related Mafic Dikes in Northern Tibet, China: Petrogenesis and Tectonic Implications. *International Geology Review*, 56(1): 57—73. <https://doi.org/10.1080/00206814.2013.818804>
- Liu, C.D., Mo, X.X., Luo, Z.H., et al., 2003. Pb-Sr-Nd-O Isotope Characteristics of Granitoids in East Kunlun Orogenic Belt. *Acta Geoscientia Sinica*, 24(6): 584—588(in Chinese with English abstract).
- Liu, Y.S., Gao, S., Hu, Z.C., et al., 2010a. Continental and Oceanic Crust Recycling-Induced Melt-Peridotite Interactions in the Trans-North China Orogen: U-Pb Dating,

- Hf Isotopes and Trace Elements in Zircons from Mantle Xenoliths. *Journal of Petrology*, 51(1–2): 537–571. <https://doi.org/10.1093/petrology/egp082>
- Liu, Y.S., Hu, Z.C., Gao, S., et al., 2008. In Situ Analysis of Major and Trace Elements of Anhydrous Minerals by LA-ICP-MS without Applying an Internal Standard. *Chemical Geology*, 257(1–2): 34–43. <https://doi.org/10.1016/j.chemgeo.2008.08.004>
- Liu, Y.S., Hu, Z.C., Zong, K.Q., et al., 2010b. Reappraisal and Refinement of Zircon U-Pb Isotope and Trace Element Analyses by LA-ICP-MS. *Chinese Science Bulletin*, 55(15): 1535–1546. <https://doi.org/10.1007/s11434-010-3052-4>
- Liu, Z.Q., Pei, X.Z., Li, R.B., et al., 2011. LA-ICP-MS Zircon U-Pb Geochronology of the Two Suites of Ophiolites at the Buqingshan Area of the A'nyemaqen Orogenic Belt in the Southern Margin of East Kunlun and Its Tectonic Implication. *Acta Geologica Sinica*, 85(2): 185–194 (in Chinese with English abstract).
- Ludwig, K.R., 2003. Isoplot 3.00: A Geochronological Toolkit for Microsoft Excel, 4. Berkeley Geochronology Center Special Publication, Berkeley.
- Luo, M.F., Mo, X.X., Yu, X.H., et al., 2014. Zircon LA-ICP-MS U-Pb Age Dating, Petrogenesis and Tectonic Implications of the Late Triassic Granites from the Xiangride Area, East Kunlun. *Acta Petrologica Sinica*, 30(11): 3229–3241 (in Chinese with English abstract).
- Luo, Z.H., Huang, Z.M., Ke, S., 2007. An Overview of Granitoid. *Geological Review*, 53(Suppl. 1): 180–226 (in Chinese with English abstract).
- Macpherson, C.G., Dreher, S.T., Thirlwall, M.F., 2006. Adakites without Slab Melting: High Pressure Differentiation of Island Arc Magma, Mindanao, the Philippines. *Earth and Planetary Science Letters*, 243(3–4): 581–593. <https://doi.org/10.1016/j.epsl.2005.12.034>
- Maniar, P.D., Piccoli, P.M., 1989. Tectonic Discrimination of Granitoids. *Geological Society of America Bulletin*, 101(5): 635–643.
- Martin, H., 1999. Adakitic Magmas: Modern Analogues of Archaean Granitoids. *Lithos*, 46(3): 411–429. [https://doi.org/10.1016/s0024-4937\(98\)00076-0](https://doi.org/10.1016/s0024-4937(98)00076-0)
- Mo, X.X., Luo, Z.H., Deng, J.F., et al., 2007. Granitoids and Crustal Growth in the East-Kunlun Orogenic Belt. *Geological Journal of China Universities*, 13(3): 403–414 (in Chinese with English abstract).
- Moyen, J.F., 2009. High Sr/Y and La/Yb Ratios: The Meaning of the “Adakitic Signature”. *Lithos*, 112(3–4): 556–574. <https://doi.org/10.1016/j.lithos.2009.04.001>
- Nowell, G.M., Kempton, P.D., Noble, S.R., et al., 1998. High Precision Hf Isotope Measurements of MORB and OIB by Thermal Ionisation Mass Spectrometry: Insights into the Depleted Mantle. *Chemical Geology*, 149(3–4): 211–233. [https://doi.org/10.1016/s0009-2541\(98\)00036-9](https://doi.org/10.1016/s0009-2541(98)00036-9)
- Patiño Douce, A.E., 1999. What do Experiments Tell Us about the Relative Contributions of Crust and Mantle to the Origin of Granitic Magmas? *Geological Society, London, Special Publications*, 168(1): 55–75. <https://doi.org/10.1144/gsl.sp.1999.168.01.05>
- Pearce, J.A., Harris, N.B.W., Tindle, A.G., 1984. Trace Element Discrimination Diagrams for the Tectonic Interpretation of Granitic Rocks. *Journal of Petrology*, 25(4): 956–983. <https://doi.org/10.1093/petrology/25.4.956>
- Prouteau, G., Scaillet, B., Pichavant, M., et al., 2001. Evidence for Mantle Metasomatism by Hydrous Silicic Melts Derived from Subducted Oceanic Crust. *Nature*, 410: 197–200. <https://doi.org/10.1038/35065583>
- Rapp, R.P., Shimizu, N., Norman, M.D., et al., 1999. Reaction between Slab-Derived Melts and Peridotite in the Mantle Wedge: Experimental Constraints at 3.8 GPa. *Chemical Geology*, 160(4): 335–356. [https://doi.org/10.1016/s0009-2541\(99\)00106-0](https://doi.org/10.1016/s0009-2541(99)00106-0)
- Rapp, R.P., Watson, E.B., 1995. Dehydration Melting of Mantabasalt at 8–32 kbar: Implications for Continental Growth and Crust-Mantle Recycling. *Journal of Petrology*, 36(4): 891–931. <https://doi.org/10.1093/petrology/36.4.891>
- Roger, F., Arnaud, N., Gilder, S., et al., 2003. Geochronological and Geochemical Constraints on Mesozoic Suturing in East Central Tibet. *Tectonics*, 22(4): 1037. <https://doi.org/10.1029/2002tc001466>
- Sen, C., Dunn, T., 1994. Dehydration Melting of a Basaltic Composition Amphibolite at 1.5 and 2.0 GPa: Implications for the Origin of Adakites. *Contributions to Mineralogy and Petrology*, 117(4): 394–409. <https://doi.org/10.1007/bf00307273>
- Shao, F.L., Niu, Y.L., Liu, Y., et al., 2017. Petrogenesis of Triassic Granitoids in the East Kunlun Orogenic Belt, Northern Tibetan Plateau and Their Tectonic Implications. *Lithos*, 282–283: 33–44. <https://doi.org/10.1016/j.lithos.2017.03.002>
- Smithies, R.H., 2000. The Archaean Tonalite-Trondhjemite-Granodiorite (TTG) Series is not an Analogue of Cenozoic Adakite. *Earth and Planetary Science Letters*, 182(1): 115–125. [https://doi.org/10.1016/s0012-821x\(00\)00236-3](https://doi.org/10.1016/s0012-821x(00)00236-3)

- Söderlund, U., Patchett, P.J., Vervoort, J.D., et al., 2004. The ^{176}Lu Decay Constant Determined by Lu-Hf and U-Pb Isotope Systematics of Precambrian Mafic Intrusions. *Earth and Planetary Science Letters*, 219(3–4): 311–324. [https://doi.org/10.1016/s0012-821x\(04\)00012-3](https://doi.org/10.1016/s0012-821x(04)00012-3)
- Song, K., Ding, Q.F., Zhang, Q., et al., 2020. Zircon U-Pb Geochronology, Hf Isotopes, and Whole-Rock Geochemistry of Hongshuihe Early to Middle Triassic Quartz Diorites and Granites in the Eastern Kunlun Orogen, NW China: Implication for Petrogenesis and Geodynamics. *Geological Journal*, 55(2): 1507–1528. <https://doi.org/10.1002/gj.3517>
- Sun, S. S., McDonough, W. F., 1989. Chemical and Isotopic Systematics of Oceanic Basalts: Implications for Mantle Composition and Processes. *Geological Society, London, Special Publications*, 42(1): 313–345. <https://doi.org/10.1144/gsl.sp.1989.042.01.19>
- Vernon, R. H., 1984. Microgranitoid Enclaves in Granites: Globules of Hybrid Magma Quenched in a Plutonic Environment. *Nature*, 309: 438–439. <https://doi.org/10.1038/309438a0>
- Wang, Y.L., Li, Y.J., Wei, J.H., et al., 2018. Origin of Late Silurian A - Type Granite in Wulonggou Area, East Kunlun Orogen: Zircon U - Pb Age, Geochemistry, Nd and Hf Isotopic Constraints. *Earth Science*, 43(4): 1219–1236(in Chinese with English abstract).
- Wang, Y.W., Wang, J.B., Long, L.L., et al., 2012. Type, Indicator, Mechanism, Model and Relationship with Mineralization of Magma Mixing: A Case Study in North Xinjiang. *Acta Petrologica Sinica*, 28(8): 2317–2330(in Chinese with English abstract).
- Wu, F., Zhang, X.J., Zhang, Y.Q., et al., 2010. Zircon U-Pb Ages for Rhyolitic Tuffs of the Naocangjiangou Formation in the East Kulun Orogenic Belt and Their Implication. *Journal of Geomechanics*, 16(1): 44–50(in Chinese with English abstract).
- Xia, R., Qing, M., Wang, C.M., et al., 2014. The Genesis of the Ore-Bearing Porphyry of the Tuoketuo Porphyry Cu-Au(Mo) Deposit in the East Kunlun, Qinghai Province: Constraints from Zircon U - Pb Geochronological and Geochemistry. *Journal of Jilin University (Earth Science Edition)*, 44(5): 1502–1524(in Chinese with English abstract).
- Xiao, W.J., Windley, B. F., Sun, S., et al., 2015. A Tale of Amalgamation of Three Permo - Triassic Collage Systems in Central Asia: Oroclines, Sutures, and Terminal Accretion. *Annual Review of Earth and Planetary Sciences*, 43: 477–507. [earth-060614-105254](https://doi.org/10.1146/annurev-<a href=)
- Xiong, F. H., 2014. Spatial - Temporal Pattern, Petrogenesis and Geological Implications of Paleo-Tethyan Granitoids in the East Kunlun Orogenic Belt (Eastern Segment) (Dissertation). China University of Geosciences, Wuhan (in Chinese with English abstract).
- Xiong, F.H., Ma, C.Q., Jiang, H.A., et al., 2016. Geochronology and Petrogenesis of Triassic High-K Calc-Alkaline Granodiorites in the East Kunlun Orogen, West China: Juvenile Lower Crustal Melting during Post-Collisional Extension. *Journal of Earth Science*, 27(3): 474–490. <https://doi.org/10.1007/s12583-016-0674-6>
- Xiong, F.H., Ma, C.Q., Zhang, J.Y., et al., 2011. LA-ICP-MS Zircon U - Pb Dating, Elements and Sr-Nd-Hf Isotope Geochemistry of the Early Mesozoic Mafic Dyke Swarms in East Kunlun Orogenic Belt. *Acta Petrologica Sinica*, 27(11): 3350–3364(in Chinese with English abstract).
- Xiong, F.H., Ma, C.Q., Zhang, J.Y., et al., 2012. The Origin of Mafic Microgranular Enclaves and Their Host Granodiorites from East Kunlun, Northern Qinghai-Tibet Plateau: Implications for Magma Mixing during Subduction of Paleo-Tethyan Lithosphere. *Mineralogy and Petrology*, 104(3–4): 211–224. <https://doi.org/10.1007/s00710-011-0187-1>
- Xiong, F.H., Ma, C.Q., Zhang, J.Y., et al., 2014. Reworking of Old Continental Lithosphere: An Important Crustal Evolution Mechanism in Orogenic Belts, as Evidenced by Triassic I-Type Granitoids in the East Kunlun Orogen, Northern Tibetan Plateau. *Journal of the Geological Society*, 171(6): 847–863. <https://doi.org/10.1144/jgs2013-038>
- Xu, J.F., Shinjo, R., Defant, M.J., et al., 2002. Origin of Mesozoic Adakitic Intrusive Rocks in the Ningzhen Area of East China: Partial Melting of Delaminated Lower Continental Crust? *Geology*, 30(12): 1111. [https://doi.org/10.1130/0091-7613\(2002\)0301111:oomair>2.0.co;2](https://doi.org/10.1130/0091-7613(2002)0301111:oomair>2.0.co;2)
- Xu, J.F., Wu, J.B., Wang, Q., et al., 2014. Research Advances of Adakites and Adakitic Rocks in China. *Bulletin of Mineralogy, Petrology and Geochemistry*, 33(1): 6–13(in Chinese with English abstract).
- Xu, Z.Q., Yang, J.S., Li, W.C., et al., 2013. Paleo-Tethys System and Accretionary Orogen in the Tibet Plateau. *Acta Petrologica Sinica*, 29(6): 1847–1860(in Chinese with English abstract).
- Yan, Z., Bian, Q.T., Korchagin, O., et al., 2008. Provenance of Early Triassic Hongshuichuan Formation in the Southern Margin of the East Kunlun Mountains: Constrains

- from Detrital Framework, Heavy Mineral Analysis and Geochemistry. *Acta Petrologica Sinica*, 24(5): 1068—1078(in Chinese with English abstract).
- Yang, J.S., Wang, X.B., Shi, R.D., et al., 2004. The Dur'ngoi Ophiolite in East Kunlun, Northern Qinghai-Tibet Plateau: A Fragment of Paleo-Tethyan Oceanic Crust. *Geology in China*, 31(3): 225—239(in Chinese with English abstract).
- Yang, J.S., Xu, Z.Q., Ma, C.Q., et al., 2010. Compound Orogeny and Scientific Problems Concerning the Central Orogenic Belt of China. *Geology in China*, 37(1): 1—11(in Chinese with English abstract).
- Yang, X.M., Sun, F.Y., Zhao, T.F., et al., 2018. Zircon U-Pb Dating, Geochemistry and Tectonic Implications of Akechukesai Gabbro in East Kunlun Orogenic Belt. *Geological Bulletin of China*, 37(10): 1842—1852(in Chinese with English abstract).
- Zhang, H.F., Chen, Y.L., Xu, W.C., et al., 2006. Granitoids around Gonghe Basin in Qinghai Province: Petrogenesis and Tectonic Implications. *Acta Petrologica Sinica*, 22(12): 2910—2922(in Chinese with English abstract).
- Zhang, J.Y., Ma, C.Q., Xiong, F.H., et al., 2012. Petrogenesis and Tectonic Significance of the Late Permian-Middle Triassic Calc-Alkaline Granites in the Balong Region, Eastern Kunlun Orogen, China. *Geological Magazine*, 149(5): 892—908. <https://doi.org/10.1017/s0016756811001142>
- Zhang, J.Y., Ma, C.Q., Xiong, F.H., et al., 2014. Early Paleozoic High-Mg Diorite-Granodiorite in the Eastern Kunlun Orogen, Western China: Response to Continental Collision and Slab Break-off. *Lithos*, 210—211: 129—146. <https://doi.org/10.1016/j.lithos.2014.10.003>
- Zhang, M.D., Ma, C.Q., Wang, L.X., et al., 2018. Subduction-Type Magmatic Rocks in Post-Collision Stage: Evidence from Late Triassic Diorite-Porphyrite of Naomuhungou Area, East Kunlun Orogen. *Earth Science*, 43(4): 1183—1206(in Chinese with English abstract).
- Zhang, Q., Jin, W.J., Xiong, X.L., et al., 2009. Characteristics and Implication of O-Type Adakite in China during Different Geological Periods. *Geotectonica et Metallogenesis*, 33(3): 432—447(in Chinese with English abstract).
- Zhang, Q., Wang, Y., Liu, H.T., et al., 2003. On the Space-Time Distribution and Geodynamic Environments of Adakites in China Annex: Controversies over Differing Opinions for Adakites in China. *Earth Science Frontiers*, 10(4): 385—400(in Chinese with English abstract).
- Zhang, Z.B., Tang, J.X., Tang, P., et al., 2019. The Origin of the Mafic Microgranular Enclaves from Jiamama Porphyry Cu Polymetallic Deposit, Tibet: Implications for Magma Mixing/Mingling and Mineralization. *Acta Petrologica Sinica*, 35(3): 934—952(in Chinese with English abstract).
- Zhang, Z.Q., Chen, J., Yu, F.C., et al., 2019. Sr-Nd-Lu-Hf Isotopic Characteristics and Geological Significance of the Middle Permian Gabbro in Xiwanggou Area, East Kunlun. *Mineralogy and Petrology*, 39(3): 26—31(in Chinese with English abstract).
- Zhao, X., Fu, L.B., Wei, J.H., et al., 2018. Geochemical Characteristics of An'nage Hornblende Gabbro from East Kunlun Orogenic Belt and Its Constraints on Evolution of Paleo-Tethys Ocean. *Earth Science*, 43(2): 354—370 (in Chinese with English abstract).
- Zhao, X., Wei, J.H., Fu, L.B., et al., 2020. Multi-Stage Crustal Melting from Late Permian Back-Arc Extension through Middle Triassic Continental Collision to Late Triassic Post-Collisional Extension in the East Kunlun Orogen. *Lithos*, 360—361: 105446. <https://doi.org/10.1016/j.lithos.2020.105446>
- Zorpi, M.J., Coulon, C., Orsini, J.B., 1991. Hybridization between Felsic and Mafic Magmas in Calc-Alkaline Granitoids: A Case Study in Northern Sardinia, Italy. *Chemical Geology*, 92(1—3): 45—86. [https://doi.org/10.1016/0009-2541\(91\)90049-w](https://doi.org/10.1016/0009-2541(91)90049-w)

附中文参考文献

- 陈国超,裴先治,李瑞保,等,2013a.东昆仑洪水川地区科鄂阿龙岩体锆石U-Pb年代学、地球化学及其地质意义.地质学报,87(2):178—196.
- 陈国超,裴先治,李瑞保,等,2013b.东昆仑造山带东段南缘和勒冈希里克特花岗岩体时代、成因及其构造意义.地质学报,87(10):1525—1541.
- 陈国超,裴先治,李瑞保,等,2018.东昆仑东段可日正长花岗岩年龄和岩石成因对东昆仑中三叠世构造演化的制约.岩石学报,34(3):567—585.
- 陈国超,裴先治,李瑞保,等,2019.东昆仑古特提斯后碰撞阶段伸展作用:来自晚三叠世岩浆岩的证据.地学前缘,26(4):191—208.
- 邓晋福,吴宗絮,杨建军,等,1995.格尔木—额济纳旗地学断面走廊域地壳—上地幔岩石学结构与深部过程.地球物理学报,38(增刊2):130—144
- 高山,章军锋,许文良,等,2009.拆沉作用与华北克拉通破坏.科学通报,54(14):1962—1973.
- 郭安林,张国伟,孙延贵,等,2007.青海省共和盆地周缘晚古生代镁铁质火山岩Sr-Nd-Pb同位素地球化学及其地质意义.岩石学报,23(4):747—754.
- 国显正,贾群子,栗亚芝,等,2016.东昆仑热水二长花岗岩地

- 球化学特征、年代学及其构造意义.矿物岩石地球化学通报,35(6):1318—1328.
- 胡朝斌,李猛,查显锋,等,2018.东昆仑祁漫塔格晚古生代末期幔源岩浆活动成因及地质意义:以鹰爪沟岩体为例.地球科学,43(12):4334—4349.
- 李瑞保,2012.东昆仑造山带(东段)晚古生代—早中生代造山作用研究(博士学位论文).西安:长安大学.
- 李瑞保,裴先治,李佐臣,等,2018.东昆仑东段古特提斯洋俯冲作用——鸟妥花岗岩体锆石 U-Pb 年代学和地球化学证据.岩石学报,34(11):3399—3421.
- 李文渊,张照伟,高永宝,等,2011.秦祁昆造山带重要成矿事件与构造响应.中国地质,38(5):1135—1149.
- 刘成东,莫宣学,罗照华,等,2003.东昆仑造山带花岗岩类 Pb-Sr-Nd-O 同位素特征.地球学报,24(6):584—588.
- 刘战庆,裴先治,李瑞保,等,2011.东昆仑南缘阿尼玛卿构造带布青山地区两期蛇绿岩的 LA-ICP-MS 锆石 U-Pb 定年及其构造意义.地质学报,85(2):185—194.
- 罗明非,莫宣学,喻学惠,等,2014.东昆仑香日德地区晚三叠世花岗岩 LA-ICP-MS 锆石 U-Pb 定年、岩石成因和构造意义.岩石学报,30(11):3229—3241.
- 罗照华,黄忠敏,柯珊,2007.花岗质岩石的基本问题.地质论评,53(增刊 1):180—226.
- 莫宣学,罗照华,邓晋福,等,2007.东昆仑造山带花岗岩及地壳生长.高校地质学报,13(3):403—414.
- 王艺龙,李艳军,魏俊浩,等,2018.东昆仑五龙沟地区晚志留世 A 型花岗岩成因:U-Pb 年代学、地球化学、Nd 及 Hf 同位素制约.地球科学,43(4):1219—1236.
- 王玉往,王京彬,龙灵利,等,2012.岩浆混合作用的类型、标志、机制、模式及其与成矿的关系——以新疆北部为例.岩石学报,28(8):2317—2330.
- 吴芳,张绪教,张永清,等,2010.东昆仑闹仓坚沟组流纹质凝灰岩锆石 U-Pb 年龄及其地质意义.地质力学学报,16(1):44—50.
- 夏锐,卿敏,王长明,等,2014.青海东昆仑托克妥 Cu-Au(Mo) 矿床含矿斑岩成因:锆石 U-Pb 年代学和地球化学约束.吉林大学学报(地球科学版),44(5):1502—1524.
- 熊富浩,2014.东昆仑造山带东段古特提斯域花岗岩类时空分布、岩石成因及其地质意义(博士学位论文).武汉:中国地质大学.
- 熊富浩,马昌前,张金阳,等,2011.东昆仑造山带早中生代镁铁质岩墙群 LA-ICP-MS 锆石 U-Pb 定年、元素和 Sr-Nd-Hf 同位素地球化学.岩石学报,27(11):3350—3364.
- 许继峰,邬建斌,王强,等,2014.埃达克岩与埃达克质岩在中国的研究进展.矿物岩石地球化学通报,33(1):6—13.
- 许志琴,杨经绥,李文昌,等,2013.青藏高原中的古特提斯体制与增生造山作用.岩石学报,29(6):1847—1860.
- 闫臻,边千韬,Korchagin, O., 等,2008.东昆仑南缘早三叠世洪水川组的源区特征:来自碎屑组成、重矿物和岩石地球化学的证据.岩石学报,24(5):1068—1078.
- 杨经绥,王希斌,史仁灯,等,2004.青藏高原北部东昆仑南缘德尔尼蛇绿岩:一个被肢解了的古特提斯洋壳.中国地质,31(3):225—239.
- 杨经绥,许志琴,马昌前,等,2010.复合造山作用和中国中央造山带的科学问题.中国地质,37(1):1—11.
- 杨锡铭,孙丰月,赵拓飞,等,2018.东昆仑阿克楚克塞地区辉长岩地球化学特征、锆石 U-Pb 年龄及其构造意义.地球通报,37(10):1842—1852.
- 张宏飞,陈岳龙,徐旺春,等,2006.青海共和盆地周缘印支期花岗岩类的成因及其构造意义.岩石学报,22(12):2910—2922.
- 张明东,马昌前,王连训,等,2018.后碰撞阶段的“俯冲型”岩浆岩:来自东昆仑瑙木浑沟晚三叠世闪长玢岩的证据.地球科学,43(4):1183—1206.
- 张旗,金惟俊,熊小林,等,2009.中国不同时代 O 型埃达克岩的特征及其意义.大地构造与成矿学,33(3):432—447.
- 张旗,王焰,刘红涛,等,2003.中国埃达克岩的时空分布及其形成背景附:《国内关于埃达克岩的争论》.地学前缘,10(4):385—400.
- 张泽斌,唐菊兴,唐攀,等,2019.西藏甲玛铜多金属矿床暗色包体岩石成因:对岩浆混合和成矿的启示.岩石学报,35(3):934—952.
- 张志青,陈静,余福承,等,2019.东昆仑希望沟中二叠世辉长岩 Sr-Nd-Lu-Hf 同位素特征及其地质意义.矿物岩石,39(3):26—31.
- 赵旭,付乐兵,魏俊浩,等,2018.东昆仑按纳格角闪辉长岩体地球化学特征及其对古特提斯洋演化的制约.地球科学,43(2):354—370.